The FATP1–DGAT2 complex facilitates lipid droplet expansion at the ER–lipid droplet interface

Ningyi Xu,[1] Shaobing O. Zhang,[1] Ronald A. Cole,[1] Sean A. McKinney,[1] Fengli Guo,[1] Joel T. Haas,[3] Sudheer Bobba,[1] Robert V. Farese Jr.,[3,4,5] and Ho Yi Mak[1, 2]

[1]Stowers Institute for Medical Research, Kansas City, MO 64110
[2]Department of Molecular and Integrative Physiology, University of Kansas Medical Center, Kansas City, KS 66160
[3]Gladstone Institute for Cardiovascular Disease, [4]Department of Medicine, and [5]Department of Biochemistry and Biophysics, University of California, San Francisco, San Francisco, CA 94158

At the subcellular level, fat storage is confined to the evolutionarily conserved compartments termed lipid droplets (LDs), which are closely associated with the endoplasmic reticulum (ER). However, the molecular mechanisms that enable ER–LD interaction and facilitate neutral lipid loading into LDs are poorly understood. In this paper, we present evidence that FATP1/acyl-CoA synthetase and DGAT2/diacylglycerol acyltransferase are components of a triglyceride synthesis complex that facilitates LD expansion. A loss of FATP1 or DGAT2 function blocked LD expansion in *Caenorhabditis elegans*. FATP1 preferentially associated with DGAT2, and they acted synergistically to promote LD expansion in mammalian cells. Live imaging indicated that FATP1 and DGAT2 are ER and LD resident proteins, respectively, and electron microscopy revealed FATP1 and DGAT2 foci close to the LD surface. Furthermore, DGAT2 that was retained in the ER failed to support LD expansion. We propose that the evolutionarily conserved FATP1–DGAT2 complex acts at the ER–LD interface and couples the synthesis and deposition of triglycerides into LDs both physically and functionally.

Introduction

Lipid droplets (LDs) are key regulatory sites for storage and mobilization of neutral lipids in response to changes in cell growth and energy demand (Farese and Walther, 2009; Goodman, 2009; Mak, 2012). Elevation of cellular fat level can be accommodated by an increase in LD size (Kuerschner et al., 2008). The sequestration of fat in the form of neutral lipids, such as triglycerides into LDs, is critical for cellular defense against lipotoxicity (Listenberger et al., 2003; Unger and Scherer, 2010). Excess free fatty acids that cannot be accommodated in LDs may cause cellular stress and insulin resistance in obese subjects. Although substantial progress has been made with regard to fat mobilization from LDs (Grönke et al., 2005; Zechner et al., 2009), the molecular mechanisms that facilitate fat deposition into LDs are poorly understood. Juxtaposition of ER and LDs has been observed in yeast and mammalian cells (Blanchette-Mackie et al., 1995; Szymanski et al., 2007; Robenek et al., 2009; Skinner et al., 2009), and it is plausible that such association may be key for coordinating lipid synthesis and cellular fat storage. However, it is unclear how ER–LD interaction is maintained in a dynamic cellular environment.

Mammalian FATP1 was originally identified as a putative fatty acid transporter (Schaffer and Lodish, 1994). Nevertheless, it possesses acyl-CoA synthetase activity (Coe et al., 1999; Hall et al., 2003) and belongs to a large family of acyl-CoA synthetases based on sequence homology. Studies in mammalian cells suggest that FATP1 may localize to the cell surface or the ER (Coe et al., 1999; Lewis et al., 2001; Stahl et al., 2002).

LD expansion may require de novo synthesis of neutral lipids, such as triglycerides, which is dependent on two DAG acyltransferases (DGATs), DGAT1 and DGAT2, in mammals (Yen et al., 2008; Harris et al., 2011). These enzymes catalyze the conjugation of a fatty acyl-CoA to DAG. Although DGAT1 and DGAT2 were originally assigned as microsomal enzymes (Cases et al., 1998; Stone et al., 2006), recent evidence suggests that DGAT2 may also localize to the LDs upon lipid loading in

Correspondence to Ho Yi Mak: hym@stowers.org

S. Bobba's present address is School of Pharmacy, University of Missouri-Kansas City, Kansas City, MO 64108.

Abbreviations used in this paper: DGAT, DAG acyltransferase; LD, lipid droplet; LRO, lysosome-related organelle; TAG, triacylglycerol.

The Rockefeller University Press $30.00
J. Cell Biol. Vol. 198 No. 5 895–911
www.jcb.org/cgi/doi/10.1083/jcb.201201139

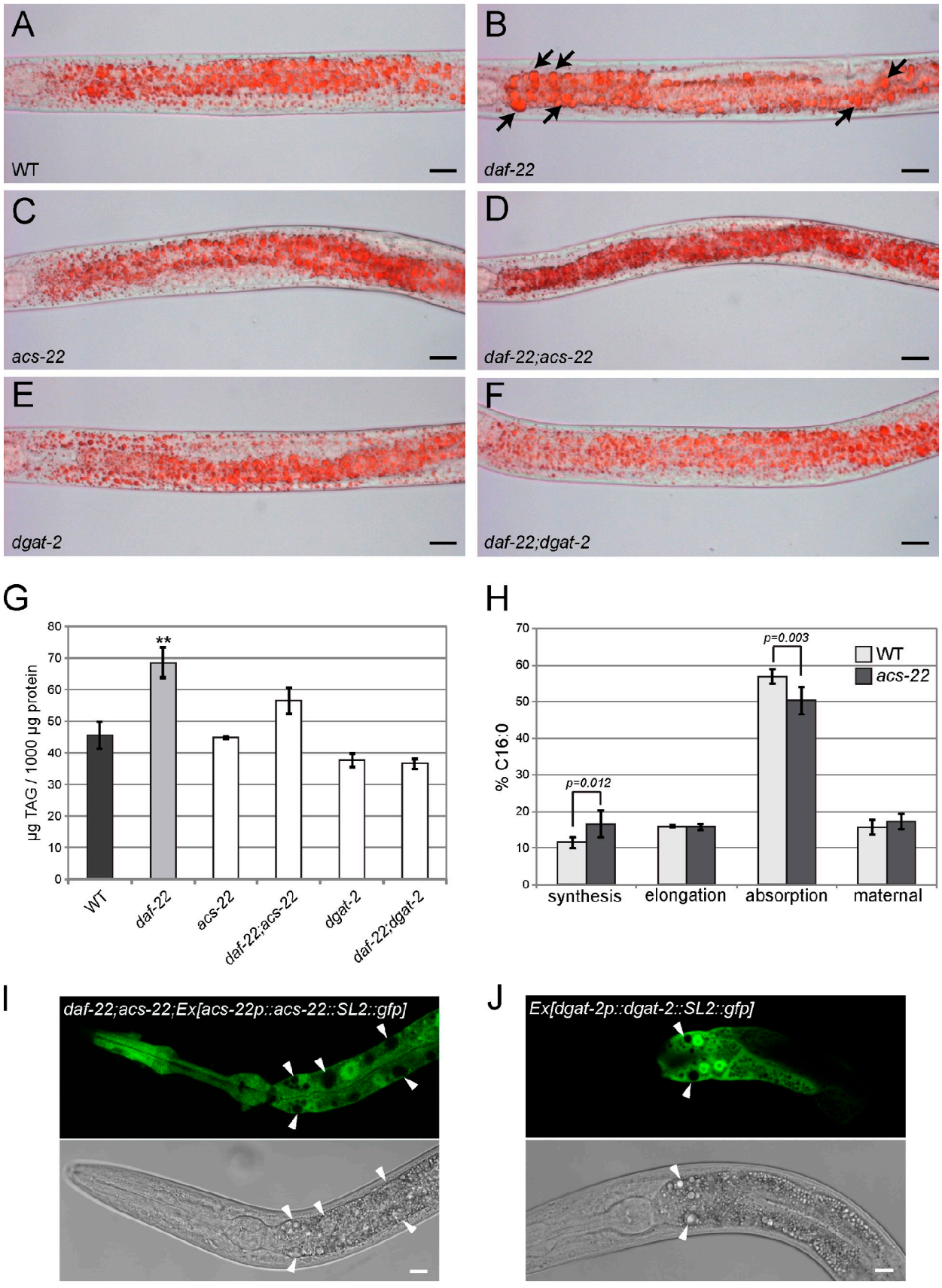

Figure 1. **ACS-22/FATP1 and DGAT-2 are required for TAG synthesis and LD expansion in *daf-22* animals.** (A–F) Oil red O staining of fixed larval stage L4 animals. Expanded LDs >3 µm in diameter (black arrows) were found in *daf-22* mutant animals (B) but were absent in wild-type (A), *acs-22* (C), *daf-22; acs-22* (D), *dgat-2* (E), and *daf-22; dgat-2* (F) animals. (G) Quantification of TAG by gas chromatography–mass spectroscopy. Synthesis of excess TAG in

mammalian cells (Kuerschner et al., 2008; Stone et al., 2009; McFie et al., 2011). Furthermore, a budding yeast orthologue of DGAT2, Dga1p, is localized to LDs (Sorger and Daum, 2002).

In this paper, we identify the *Caenorhabditis elegans* orthologues of FATP1 and DGAT2 as genetic regulators of LD expansion. Biochemical, imaging, and functional analysis revealed that FATP1 and DGAT2 form a conserved protein complex at the ER–LD interface to promote LD expansion. Our results suggest one mechanism for triacylglycerol (TAG) synthesis and channeling that links ER and LD through a macromolecular complex.

Results

ACS-22/FATP1 is required for LD expansion

To identify genes that are required for LD expansion in an unbiased manner, we performed a genetic suppressor screen in a *daf-22* mutant background. We have previously shown that animals lacking DAF-22, the terminal thiolase for peroxisomal fatty acid β oxidation in *C. elegans*, accumulate excess triglycerides in expanded LDs that are >3 µm in diameter (Zhang et al., 2010a). We mutagenized *daf-22(ok693)* animals with ethyl methanesulfonate and recovered >15 independent mutant alleles that suppressed the LD expansion phenotype. Here, we report the cloning of *acs-22* and *dgat-2*. We isolated four recessive and one semidominant alleles of *acs-22* and determined that the *hj25* and *hj26* alleles are molecular nulls (Fig. S1). The *acs-22* gene encodes a very long chain fatty acyl-CoA synthetase, which is orthologous to mammalian FATP1 and FATP4 (Schaffer and Lodish, 1994; Stahl et al., 1999). It has been reported that *acs-22* is required for cuticle integrity in *C. elegans* (Kage-Nakadai et al., 2010). The loss of *acs-22* function suppressed LD expansion in *daf-22* mutant animals and reduced their TAG content (Fig. 1, D and G; and Fig. 2, B and G, bar 2). In comparison with wild-type animals, the TAG levels of *daf-22* and *daf-22; acs-22* animals were elevated by 50 and 24%, respectively (Fig. 1 G). ACS-22 is specifically required for LD expansion in *daf-22* animals because individual knockdown of 20 other *acs* (*acyl-CoA synthetase*) gene family members by RNAi did not block LD expansion in *daf-22* animals (Table S1). However, ACS-22 was not required for LD biogenesis or triglyceride synthesis in otherwise wild-type animals (Fig. 1, C and G). Our results suggest that other acyl-CoA synthetases may act redundantly to fulfill these functions because individual knockdown of other *acs* genes did not detectably impair animal growth and development (Table S1). We detected GFP expression in the intestine, pharynx, excretory cell, vulval muscle, and anal muscle in animals carrying a rescuing bicistronic transgene that directs GFP expression under the control of the *acs-22* 5′ regulatory region and its open reading frame (Fig. 1 I). Genetic mosaic and tissue-specific rescue experiments indicated that ACS-22 acts cell autonomously in the intestine to facilitate LD expansion (Fig. S2).

We determined that ACS-22 is a functional orthologue of mammalian FATP1 because transgenic expression of mouse FATP1 restores LD expansion in *daf-22; acs-22* mutant animals (Fig. S3 E). Using the ^{13}C isotope labeling technique (Perez and Van Gilst, 2008), we found that C16:0 fatty acid absorption in wild-type and *acs-22(hj26)*–null animals differed by 6% (Fig. 1 H). Therefore, ACS-22 is not essential for fatty acid uptake in *C. elegans*. Our genetic evidence indicates that the acyl-CoA synthetase activity is necessary for ACS-22 to facilitate LD expansion. The semidominant *hj36* allele encodes a D496N substitution, which did not affect the expression level of ACS-22 (Fig. S1). The D496 residue is conserved in mammalian FATP1, and it is required for the catalytic activity of acyl-CoA synthetases for its binding to the AMP moiety of fatty acyl-AMP, an intermediate in the conversion of fatty acid to fatty acyl-CoA (Hisanaga et al., 2004). Overexpression of ACS-22 (D496N) interfered with wild-type ACS-22 function and inhibited LD expansion in *daf-22* mutant animals (Fig. 2 G, bar 5; and Fig. S3 A). Because FATP1 can form oligomers (Richards et al., 2003), it is conceivable that mutant ACS-22 binds to wild-type ACS-22 to form defective oligomers that fail to yield acyl-CoA precursors for triglyceride synthesis. An unbiased forward genetic screen followed by targeted sequencing of the *acs-22* coding region revealed 13 additional conserved residues that are critical for ACS-22 stability or function (Fig. S1, A and C). Notably, mutation at the ATP-binding P loop (G253S) or the highly conserved L motif for intramolecular interaction (D510N) did not affect protein stability (Fig. S1 C) or localization (Fig. S3, G and H) but abolished the ability of mutant ACS-22 to support LD expansion in *daf-22*(−) animals (Fig. S3, I and J). These results provide further support that the acyl-CoA synthetase activity of ACS-22 is necessary for LD expansion.

DGAT-2 is required for LD expansion

We hypothesized that ACS-22/FATP1 might act cooperatively with a triglyceride synthesis enzyme to support LD expansion in *daf-22* mutant animals. Sequence analysis using mammalian DGAT2 (Cases et al., 2001), a key enzyme for triglyceride synthesis, identified four putative *C. elegans* orthologues. To test whether any of these proteins were regulators of LD size, we knocked down W01A11.2, K07B1.4, Y53G8B.2, and F59A1.10 individually by RNAi and found that F59A1.10 was uniquely required for LD expansion in *daf-22* mutant animals. Accordingly, we isolated a single missense allele of F59A1.10 from a

daf-22 mutant animals required ACS-22/FATP1 and DGAT-2. Results were means ± SEM of measurements from three to six independent populations of animals of each genotype. In a pairwise *t* test, $P < 0.05$ between wild-type (WT) and *daf-22* samples (asterisks); $P > 0.1$ between WT and all other samples. (H) Quantitation of palmitic acid (C16:0) absorption, synthesis, elongation, and maternal deposition by ^{13}C isotope labeling. Results were means ± SEM from six independent populations of each strain of animals. (I) The *acs-22* gene is expressed in multiple tissues including the intestine. The bicistronic *acs-22p::acs-22::SL2::gfp* transgene, which expressed ACS-22 and GFP independently under the control of the *acs-22* promoter, rescued the loss of *acs-22* function and restored expanded LD (white arrowheads) in *daf-22; acs-22* mutant animals. An L4 animal is shown. (J) The *dgat-2* gene is expressed in the intestine. Overexpression of *dgat-2* was sufficient for promoter LD expansion in wild-type animals. An L4 animal is shown. Bars: (A–F) 20 µm; (I and J) 10 µm.

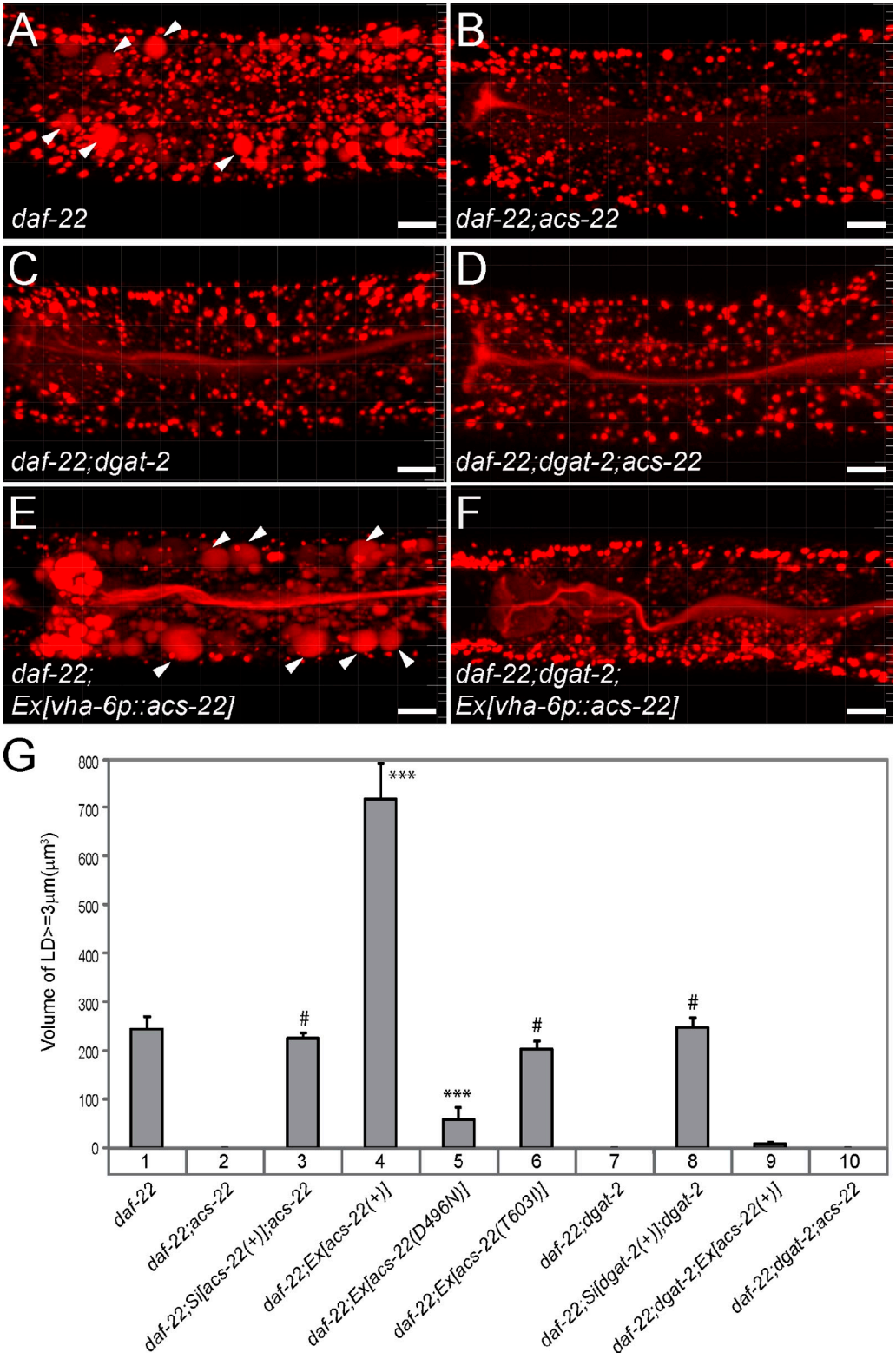

Figure 2. **ACS-22/FATP1 and DGAT-2 act in the same genetic pathway.** (A–F) Red BODIPY-C12 staining of larval stage L4 animals. Expanded LDs >3 µm in diameter were indicated by white arrowheads. Images were 3D projections of 9-µm confocal z stacks that covered the first three intestinal segments. Bars, 10 µm. (G) Quantification of total volumes of BODIPY-positive structures that were >3 µm in diameter in the second intestinal segment of larval stage L4 animals. For each strain, a total of 20 animals were imaged at two independent times, except for *daf-22; hjSi29[acs-22(+)]; acs-22* (n = 17) and *daf-22; hjSi56[dgat-2(+)]; dgat-2* (n = 16). For experiments using extrachromosomal arrays, two independent transgenic lines were quantified, with 10 animals each. Data were plotted as means ± SEM. Pairwise t test between lane 1 and lanes 3, 6, or 8: #, $P > 0.1$. Pairwise t test between lane 1 and lanes 2, 4, 5, 7, 9, or 10: ***, $P < 0.001$.

daf-22 suppressor screen and renamed the gene *dgat-2*. Similar to ACS-22, loss of *dgat-2* function prevented LD expansion in *daf-22* mutant animals and reduced their triglyceride content to wild-type levels (Fig. 1, F and G; and Fig. 2, C and G, bar 7). We detected GFP expression in the intestine in animals carrying a bicistronic transgene that directs GFP expression under the control of the *dgat-2* 5′ regulatory region and its open reading frame (Fig. 1 J). Overexpression of DGAT-2 from this transgene not only restored LD expansion in *daf-22; dgat-2* mutant animals, it was sufficient to drive LD expansion in wild-type animals (Fig. 1 J). In contrast, overexpression of ACS-22 failed to promote LD expansion in wild-type animals. Our results suggest that *dgat-2* is limiting in wild-type animals, and its expression level is tightly regulated. Transgenic expression of mouse DGAT2 restored LD expansion in *daf-22; dgat-2* mutant animals, indicating that DGAT-2 is indeed the functional orthologue of mammalian DGAT2 (Fig. S3 F). We noted that the basal triglyceride level was not significantly affected in *dgat-2* mutant animals (Fig. 1 G), suggesting that at least one other DGAT-related enzyme substitutes for DGAT-2 in triglyceride synthesis. Indeed, the *C. elegans* genome also encodes a putative orthologue of mammalian DGAT1 (H19N07.4; Cases et al., 1998).

FATP1 and DGAT2 form a protein complex for LD expansion

We propose that ACS-22 acts as an acyl-CoA synthetase to generate acyl-CoA, which is then conjugated to DAG for triglyceride synthesis by DGAT-2. Our model predicts that ACS-22 and DGAT-2 may form a stable complex to allow the transfer of acyl-CoA from ACS-22 to DGAT-2. We tested this hypothesis by first asking whether ACS-22 and DGAT-2 could physically associate with each other when they were coexpressed in mammalian cells. We found that ACS-22 coimmunoprecipitated with DGAT-2 but not the YFP Venus (Fig. 3 A). Next, we tested whether mouse FATP1 and DGAT2 could also associate with each other. Although DGAT2 could only be expressed at a low level (undetectable in Fig. 3 C [lane 2] as 10% input and weakly detectable in Fig. 3 C [lane 6] after enrichment by immunoprecipitation), we found that FATP1 strongly associated with DGAT2 (Fig. 3 C, lane 6). In contrast, little FATP1 was recovered by coimmunoprecipitation with the highly expressed DGAT1, which served as a control for nonspecific binding to membrane-associated proteins (Fig. 3 C, lane 5). In addition, the YFP Venus failed to associate with FATP1 (Fig. 3 C, lane 7), whereas FATP1 was able to associate with itself as previously reported (Fig. 3 C, lane 8; Richards et al., 2003). Therefore, FATP1–DGAT2 interaction was specific under our experimental conditions. We next asked whether the FATP1–DGAT2 interaction was dependent on the catalytic activity of FATP1. To this end, we generated mutant forms of FATP1 that had no ATPase activity (S250A; Stuhlsatz-Krouper et al., 1998) or carried amino acid substitutions at conserved residues that were mutated in *acs-22(hj23)* and *acs-22(hj36)* mutant worms (T596I and D492N, respectively). Coimmunoprecipitation experiments indicated that FATP1 function was not necessary for its association with DGAT2 (Fig. 3 D).

To test whether FATP1 and DGAT2 could interact directly, we translated both proteins in vitro using reticulocyte lysates and subjected them to coimmunoprecipitation assays. FATP1 associated with DGAT2 but not the negative control Venus YFP (Fig. 3 E, lanes 4 and 5). We also generated a mutant DGAT2 that was catalytically dead (H163A; Stone et al., 2006) and noted that the H163A mutation did not appreciably affect its association with FATP1 in vitro (Fig. 3 E, lane 6). To further define the regions in FATP1 and DGAT2 that are necessary for their interaction, we generated a series of deletion mutants. By coimmunoprecipitation of in vitro translated proteins, we determined that the central region of DGAT2 (amino acids 116–228) but not its N terminus is sufficient for interaction with FATP1 (Fig. 3 F, compare lane 8 with lane 6). We also found that FATP1 (amino acids 191–313) was sufficient for direct interaction with DGAT2 (Fig. 3 G, lane 10). An overlapping region of FATP1 (amino acids 101–257) served as the negative control (Fig. 3 G, land 9). Our results indicate that FATP1 and DGAT2 form a protein complex in vitro and in vivo.

In addition to physical interaction, genetic evidence lends further support that *acs-22* and *dgat-2* act in the same pathway. Loss of either *acs-22* or *dgat-2* function suppressed LD expansion in *daf-22*(−) animals, and loss of *dgat-2* function in *daf-22; acs-22* mutant animals did not alter the degree of suppression or cause synthetic phenotypes (Fig. 2, D and G, bar 10). Furthermore, overexpression of ACS-22 in *daf-22* mutant animals strongly promoted LD expansion that was strictly dependent on DGAT-2 function (Fig. 2, E–G, bars 4 and 9). Collectively, our results suggest that FATP1 and DGAT2 are physically and functionally coupled as part of a triglyceride synthesis complex that facilitates LD expansion.

ACS-22/FATP1 and DGAT2 are ER and LD resident proteins, respectively

Mammalian FATP1 was reported to localize to the ER or cell surface (Coe et al., 1999; Lewis et al., 2001; Stahl et al., 2002), whereas DGAT2 was shown to be an ER protein that could relocate to the proximity of LDs upon lipid loading in fixed mammalian cells (Kuerschner et al., 2008; Stone et al., 2009; McFie et al., 2011). No live-imaging experiments have been reported to date. To determine the subcellular localization and dynamics of ACS-22/FATP1 and DGAT-2 in live animals, we expressed low levels of functional ACS-22::GFP, GFP::DGAT-2, and mRuby::DGAT-2 fusion proteins from rescuing single-copy transgenes (Fig. 2 G, bars 3 and 8; and Fig. S3, C and D). We also generated transgenic animals that expressed an ER resident signal peptidase fused to GFP or mKO2 (GFP::SP12 or mKO2::SP12; Rolls et al., 2002). In wild-type animals, mKO2::SP12 and GFP::SP12 illuminate the nuclear envelope and a reticular tubular network that extends to the cell cortex of intestinal cells (Fig. 4 B and Fig. S4 B), which closely resembles the ER architecture observed in yeast and mammalian cells (Voeltz et al., 2002). We found that the subcellular localization of ACS-22::GFP fusion protein was indistinguishable from mKO2::SP12 (Fig. 4, A–C). In FRAP experiments, the lifetime of ACS-22::GFP and GFP::SP12 was comparable (Fig. 5 H and Fig. S4), strongly suggesting that ACS-22::GFP is a resident ER protein in *C. elegans.*

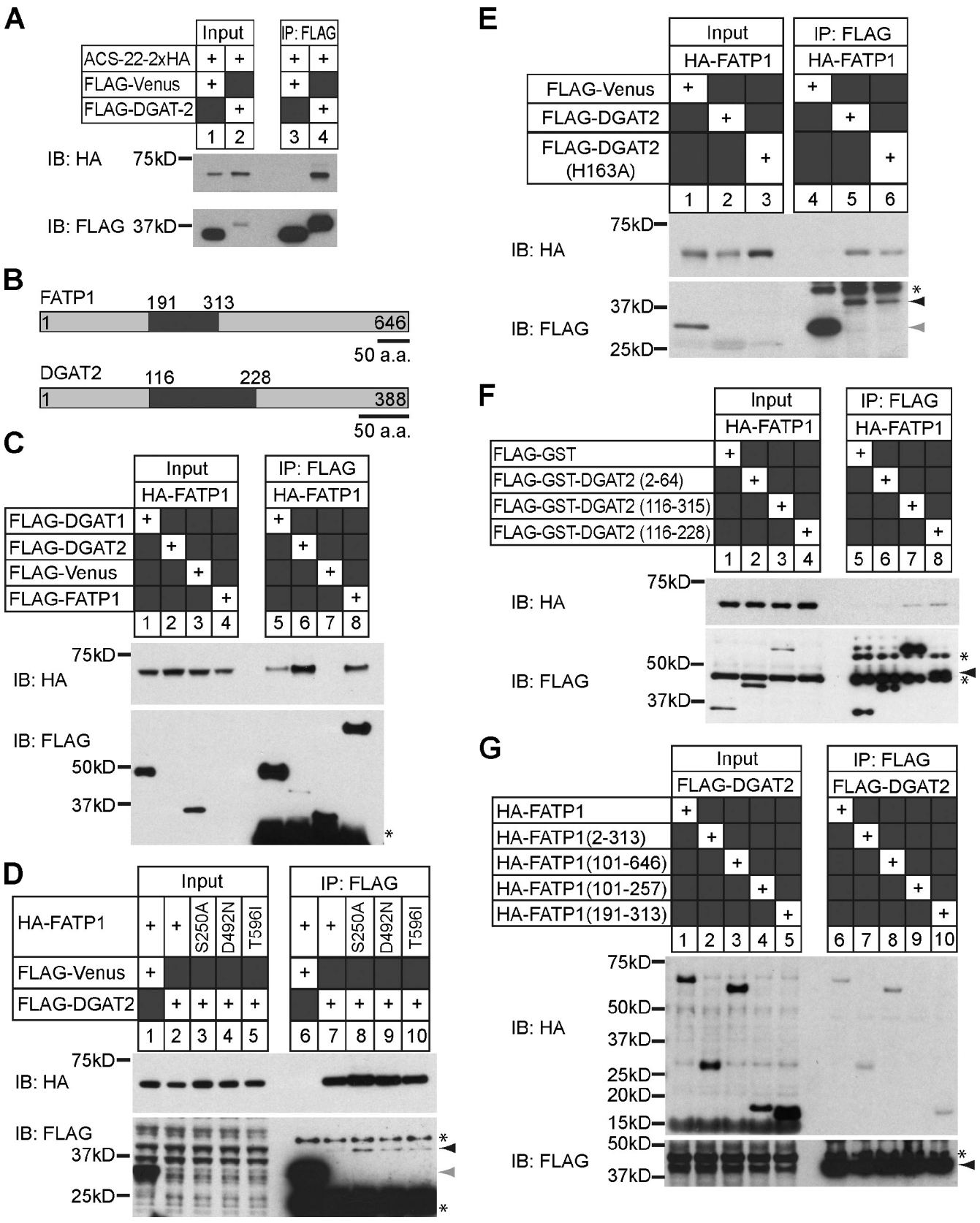

Figure 3. **Physical interaction between mammalian FATP1 and DGAT2.** (A) ACS-22–2×HA coimmunoprecipitated with FLAG-DGAT-2 from HEK293T cell extracts. 6% input of each sample was loaded. (B) Schematic representation of mouse FATP1 and DGAT2 proteins. Minimal regions that are required for FATP1–DGAT2 interaction are shaded in dark gray. (C) HA-FATP1 preferentially coimmunoprecipitated with FLAG-DGAT2 from HeLa cell extracts. FLAG-DGAT1 was expressed at very high level, yet showed weaker association with HA-FATP1. HA-FATP1 also associated with FLAG-FATP1 but not FLAG-Venus. 5% input of each sample was loaded for HA-FATP1, and 10% input of each sample was loaded for FLAG-tagged proteins. The input of FLAG-DGAT2

In contrast to ACS-22::GFP, the GFP::DGAT-2 fusion protein was localized to spherical structures <2 µm in diameter in wild-type intestinal cells (Fig. 4 D). Such localization was independent of the fluorescent protein fusion partner because mRuby::DGAT-2 also localized to similar structures (Fig. 5 B). These structures may represent LDs or lysosome-related organelles (LROs) that contain autofluorescent material (Schroeder et al., 2007; Zhang et al., 2010b). We performed live imaging in λ mode followed by linear unmixing, which clearly indicated that GFP::DGAT-2 was absent from the surface of autofluorescent LROs (Fig. 4, D–G). In FRAP experiments, GFP::DGAT-2 failed to recover within 200 s after photobleaching, in contrast to the dynamic movement of ACS-22::GFP within the ER in wild-type animals (Fig. S4). Therefore, we conclude that GFP::DGAT-2 is a LD resident protein. Our results also imply that the LD targeting of GFP::DGAT-2 cannot be achieved by rapid lateral diffusion from membrane structures, such as the ER, suggesting that the ER and LDs are unlikely to be contiguous in *C. elegans* intestinal cells.

Preferential enrichment of ACS-22/FATP1 at the ER–LD interface

In *daf-22* mutant animals, LDs undergo continual expansion throughout development (Zhang et al., 2010a). In these animals, ACS-22::GFP was observed in reticular structures and appeared to envelop expanded LDs (Fig. 5 D). This is consistent with ultrastructural evidence that the ER closely associates with LDs, especially under lipid loading conditions (Blanchette-Mackie et al., 1995; Robenek et al., 2009). Several lines of evidence indicate preferential enrichment of ACS-22::GFP at the ER–LD interface during LD expansion in *daf-22(−)* animals. First, ACS-22::GFP showed significantly higher degree of colocalization with mRuby::DGAT-2 than another ER resident protein, GFP::SP12 (Fig. 5, F and G). Second, ACS-22::GFP at the ER–LD interface recovered significantly less than GFP::SP12 after photobleaching in FRAP experiments ($P < 0.0001$ at 33 s after bleach, *t* test; Fig. 6, A–G). This observation indicates that ACS-22::GFP is less mobile than GFP::SP12 and suggests that ACS-22 is engaged in a stable protein complex. Third, we found ACS-22::GFP and GFP::DGAT-2 fusion proteins in discrete foci at or near the LD surface in *daf-22* mutant animals by immunoelectron microscopy (Fig. 6, I and J). Collectively, our results are consistent with a model that ACS-22/FATP1 and DGAT-2 form a complex at the ER–LD interface to support LD expansion.

DGAT-2 acts at LDs to promote LD expansion

Although mammalian DGAT2 had been found on LD surface in cultured cells under lipid loading conditions (Kuerschner et al., 2008; Stone et al., 2009), it was unclear whether this was necessary for DGAT2 to support LD expansion. We directly tested this hypothesis by appending the ER-anchoring region of mouse cytochrome b5 (residues 100–134; Honsho et al., 1998) to the C terminus of *C. elegans* DGAT-2 and asked whether the fusion protein could substitute for wild-type DGAT-2 function. The cb5-anchoring region had been shown to retain heterologous proteins to the ER (Zhu et al., 1996), and the GFP::DGAT-2::cb5 fusion protein expressed from a single-copy transgene was indeed localized to the ER (Fig. 7 A). More importantly, expression of GFP::DGAT-2::cb5 failed to restore LD expansion in *daf-22; dgat-2* mutant animals (Fig. 7, B and E, bar 3). To demonstrate that the cb5 anchor did not interfere with DGAT-2 function per se, we introduced four charged residues in the hydrophobic transmembrane domain of cb5 (Fig. 7 C). Disruption of ER anchoring in GFP::DGAT-2::$cb5_{mut}$ fusion protein partially restored LD localization and its ability to support LD expansion (Fig. 7, D and E, bar 4). To measure the catalytic activity of various DGAT2 mutant proteins, we expressed them in a yeast strain (Δ4) that could not synthesize TAG (Sandager et al., 2002). The DGAT activity of cell extracts from yeast expressing mRuby::DGAT2, mRuby::DGAT2::cb5, or mRuby::DGAT2::$cb5_{mut}$ proteins was comparable (Fig. 7 F, lanes 3–5). This result confirmed that the cb5-anchoring region did not interfere with the catalytic activity of DGAT2. Collectively, our results suggest that LD localization of DGAT-2, which allows direct deposition of its TAG product into LDs, is critical for LD expansion.

Mammalian FATP1 and DGAT2 act in concert to promote LD expansion

Because ACS-22/FATP1 and DGAT-2 are highly conserved in mammals, our model predicts that FATP1 and DGAT2 should cooperate to promote LD expansion in mammalian cells. We transiently expressed FATP1::Venus, Venus::DGAT2, or mRuby::DGAT2 fusion proteins in COS7 cells and monitored their localization after oleic acid loading. We found FATP1::Venus at the ER (Fig. 8 A) and Venus::DGAT2 and mRuby::DGAT2 at LDs (Fig. 8 B and Fig. S5 B) consistent with previous studies (Coe et al., 1999; Kuerschner et al., 2008; Stone et al., 2009; McFie et al., 2011). Furthermore, mRuby::DGAT2 colocalized with Perilipin2::GFP on the LD surface (Fig. S5). Coexpression

(lane 2) was not detectable because of its low level of expression. The asterisk indicates immunoglobulin light chains. (D) FLAG-DGAT2 (black arrowhead) associated with wild-type and mutant HA-FATP1 with similar affinity in HEK293T cell extracts. FLAG-Venus was indicated by the gray arrowhead. 5% input of each sample was loaded for HA-FATP1, and 10% input of each sample was loaded for FLAG-tagged proteins. The FLAG-DGAT2 signal was obscured by background signals in lanes 2–5. The asterisks indicate immunoglobulin light chains and a nonspecific protein larger than DGAT2 in lanes 6–10. (E) Coimmunoprecipitation of in vitro translated HA-FATP1 with FLAG-DGAT2 (black arrowhead) but not FLAG-Venus (gray arrowhead). 3% input of each sample was loaded for HA-FATP1, and 13% input of each sample was loaded for FLAG-tagged proteins. The asterisk indicates a nonspecific protein. (F) Coimmunoprecipitation of in vitro translated HA-FATP1 with deletion mutants of FLAG-GST-DGAT2. 1.4% input of each sample was loaded for HA-FATP1, and 28% input of each sample was loaded for FLAG-tagged proteins. The asterisk indicates nonspecific proteins. The black arrow indicates FLAG-GST-DGAT2(116–228) that partially overlaps with a nonspecific band. (G) Coimmunoprecipitation of in vitro translated HA-FATP1 deletion mutants with FLAG-DGAT2 (black arrowhead). 1.4% input of each sample was loaded for HA-FATP1, and 56% input of each sample was loaded for FLAG-tagged proteins. The asterisk indicates a nonspecific protein. IB, immunoblotting; IP, immunoprecipitation.

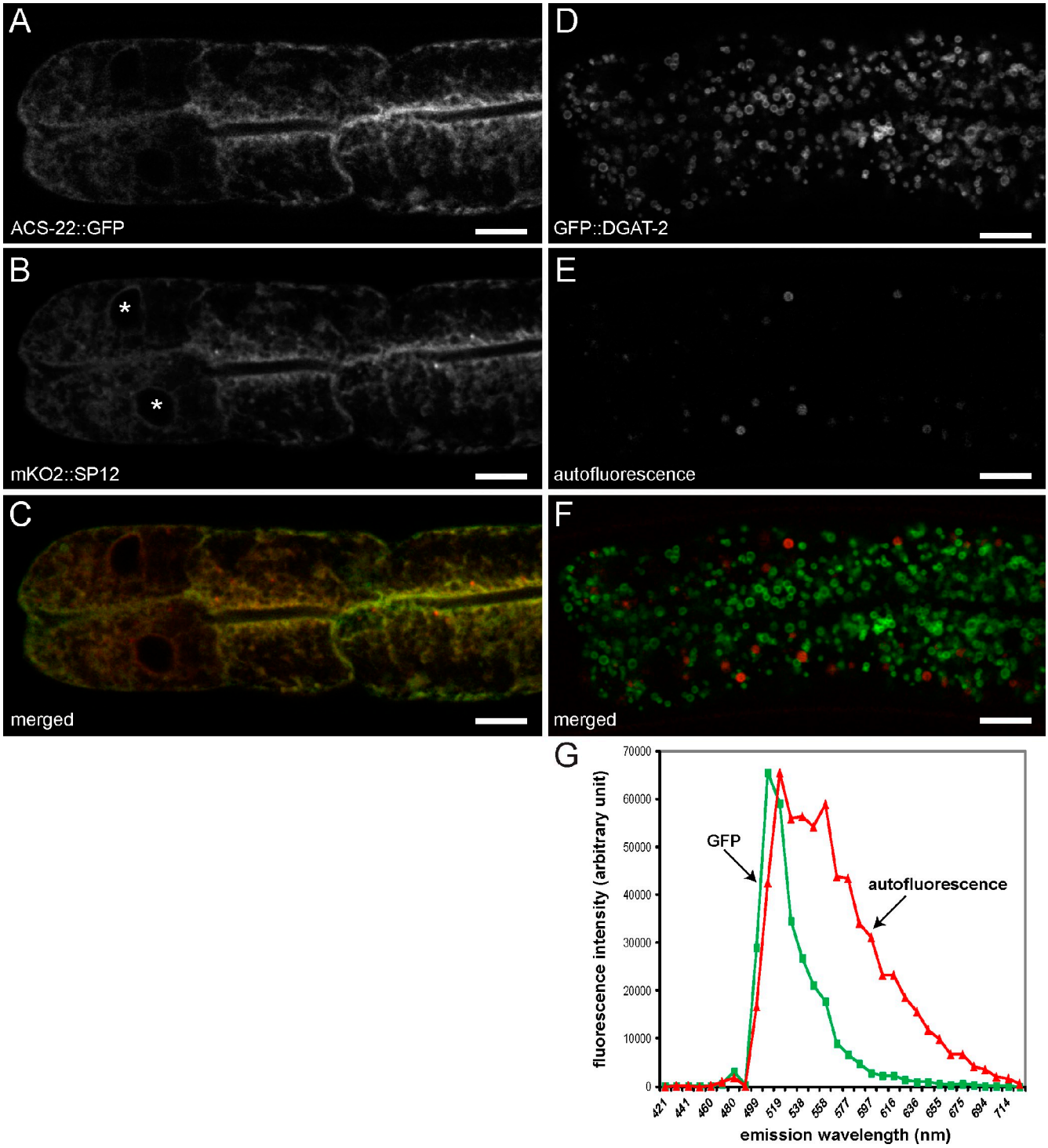

Figure 4. **ACS-22::GFP and GFP::DGAT-2 are ER and LD resident proteins, respectively.** (A–C) Colocalization of ACS-22 with the ER resident protein signal peptidase SP12. Representative images of a larval stage L4 animal carrying single-copy transgenes *hjSi29[vha-6p::acs-22::gfp]* and *hjSi61[vha-6p::mKO2::sp12]*. The ACS-22::GFP and mKO2::SP12 fusion proteins colocalized at the ER. Asterisks indicate the position of nuclei. (D–F) GFP::DGAT-2 did not localize to autofluorescent LROs. Representative images of an animal at larval stage L4 carrying the *hjSi56[vha-6p::gfp::dgat-2]* transgene. Confocal images were obtained in λ mode using a 488-nm excitation laser followed by linear unmixing. Autofluorescence was pseudocolored red. (G) Reference spectra of GFP (green) and autofluorescence (red) used for linear unmixing. Bars, 10 µm.

of FATP1::Venus and mRuby::DGAT2 under the same conditions strongly promoted LD expansion (Fig. 8, C and F). In addition to ER localization, FATP1::Venus was also enriched around LDs that were marked by mRuby::DGAT2 (Fig. 8 C). The functional synergy between FATP1 and DGAT2 in promoting LD expansion was dependent on their respective catalytic activities (Fig. 8 F). Interestingly, the catalytically dead mRuby::DGAT2 (H163A) mutant protein failed to localize to the LD surface (Fig. 8 E). Extensive colocalization of DGAT2 (H163A) with FATP1 in the ER did not significantly affect their affinity to

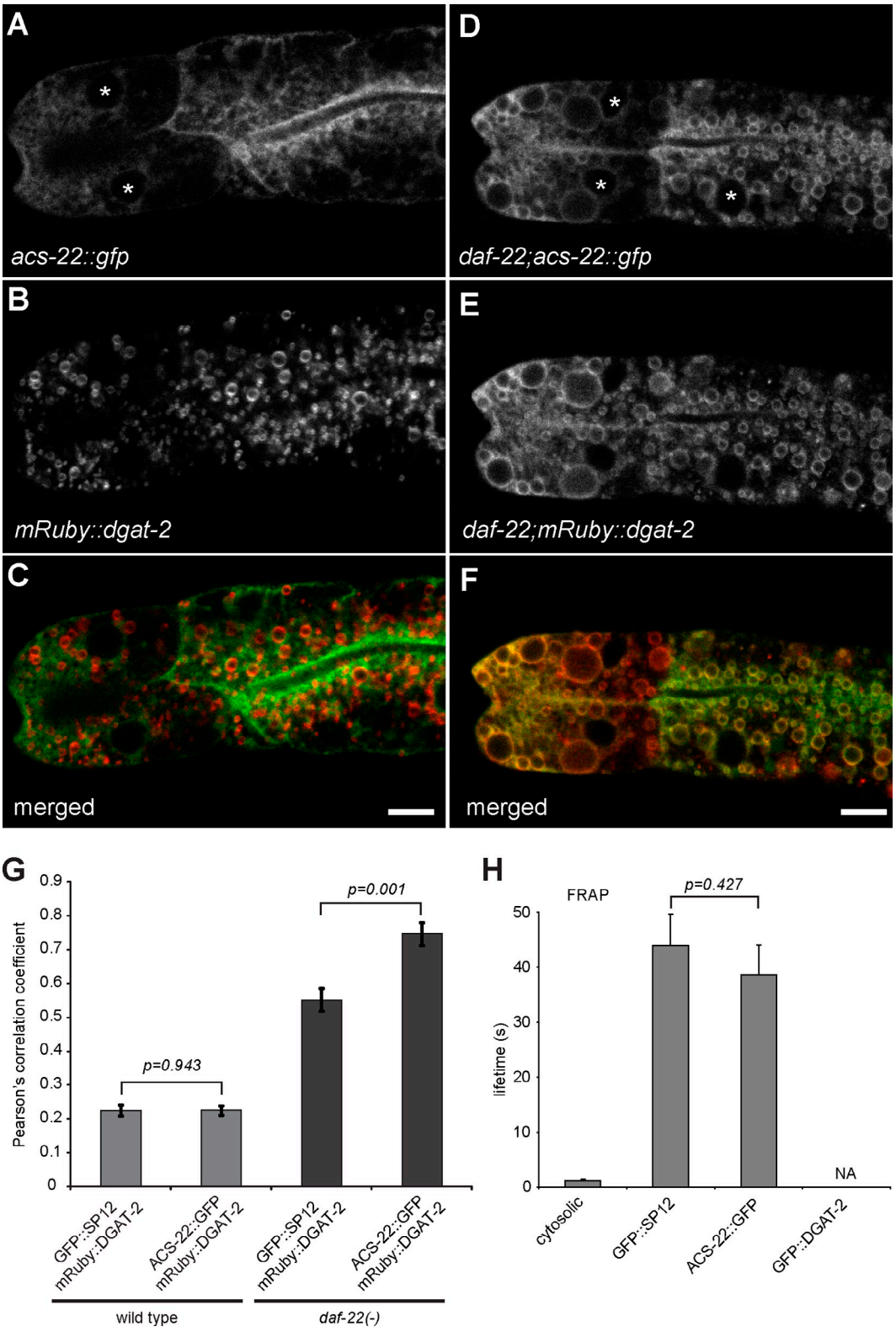

Figure 5. **ACS-22/FATP1 and DGAT-2 are ER and LD resident proteins, respectively.** (A–F) Representative confocal images of larval L4 stage animals carrying single-copy transgenes that express ACS-22::GFP (*hjSi29*) and mRuby::DGAT-2 (*hjSi62*) fusion proteins in wild-type (A–C) or *daf-22* mutant animals (D–F). Asterisks indicate the position of nuclei. Bars, 10 µm. (G) Preferential colocalization of ACS-22::GFP with mRuby::DGAT2 in *daf-22* animals. Pearson's correlation coefficients of ACS-22::GFP with mRuby::DGAT-2 fluorescent signals and GFP::SP12 with mRuby::DGAT-2 fluorescent signals in wild-type (n = 10) and *daf-22* (n = 7, ACS-22::GFP; n = 8, GFP::SP12) animals are shown. Data were plotted as means ± SEM. P-values are obtained from pairwise t test. (H) FRAP experiments indicate that ACS-22 is a resident ER protein. The fluorescence recovery lifetime of ACS-22::GFP fusion protein is shown in comparison to that of cytosolic GFP (cytosolic) and GFP::SP12 (ER) control proteins. There is no statistically significant difference between the lifetime of ACS-22::GFP and GFP::SP12 proteins. The GFP::DGAT-2 fusion protein did not recover 200 s after photobleaching, and therefore, a fluorescence recovery lifetime measurement is not applicable (NA). Number of independent photobleaching events: cytosolic = 12; GFP::SP12 = 11; ACS-22::GFP = 10; GFP::DGAT-2 = 8. Data were plotted as means ± SEM. P-value from t test is shown.

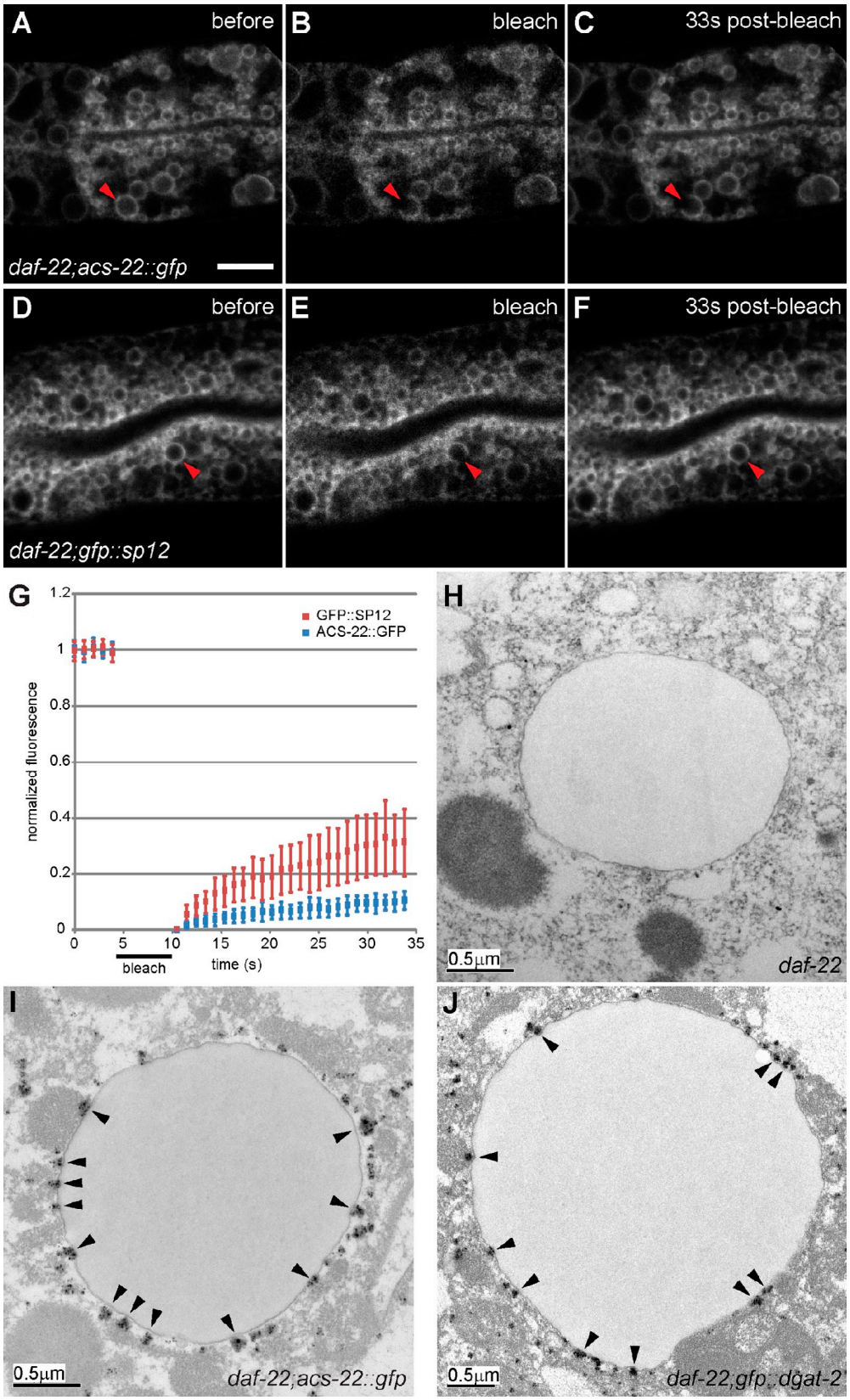

Figure 6. **Enrichment of ACS-22::GFP at the ER–LD interface.** (A–G) Reduced mobility of ACS-22::GFP in comparison to GFP::SP12 at the ER–LD interface. Representative confocal images of larval L4 stage *daf-22* animals expressing ACS-22::GFP (A–C) or GFP::SP12 (D–F) in FRAP experiments. Red arrowheads marked photobleached area (2 µm in diameter). Bar, 10 µm. (G) Normalized fluorescence of ACS-22::GFP and SP12::GFP. Number of independent photobleaching events: ACS-22::GFP = 22; GFP::SP12 = 19. Data were plotted as means ± SD. (H–J) Electron micrographs showing clusters of ACS-22::GFP (I) or GFP::DGAT-2 (J) fusion protein at or near the LD surface in *daf-22* animals. Fusion proteins were visualized by immunogold labeling followed by silver enhancement. Black arrowheads indicate electron-dense clusters. Bars, 0.5 µm.

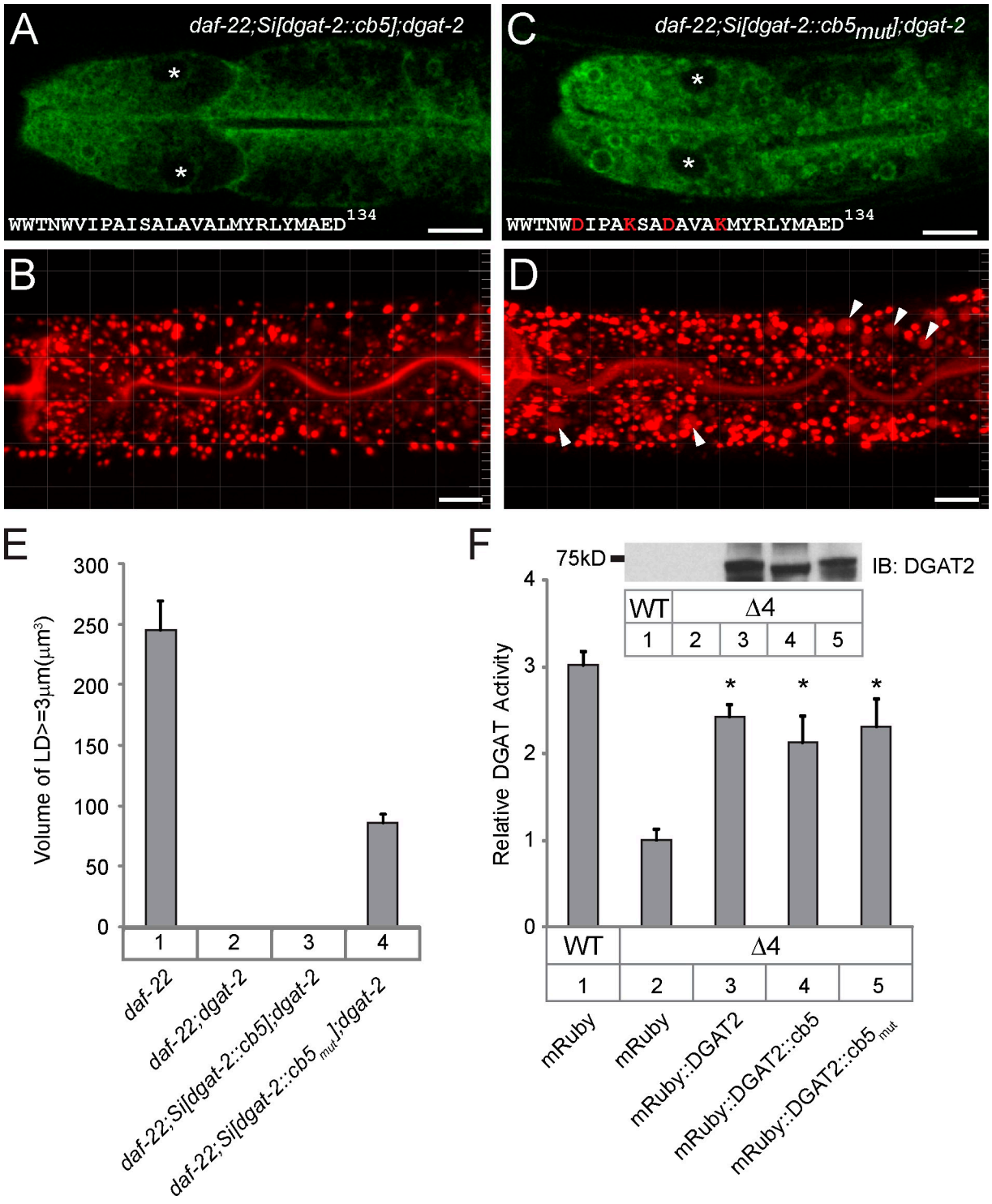

Figure 7. **LD targeting of DGAT-2 is critical for its function.** (A and B) The single-copy transgene *hjSi76[vha-6p::gfp::dgat-2::cb5]* expressed the ER-tethered GFP::DGAT-2::cb5 fusion protein at physiological levels and failed to restore LD expansion in *daf-22(ok693); dgat-2(hj44)* mutant animals. (A) A representative image showing ER localization of GFP. Asterisks indicate the position of nuclei. The wild-type cb5 C-terminal sequence is shown. (B) Red BODIPY-C12 staining of a representative larval stage L4 animal. Imaging conditions are identical to that used in Fig. 2. (C and D) The single-copy transgene *hjSi87[vha-6p::gfp::dgat-2::cb5$_{mut}$]* partially supported LD expansion in *daf-22(ok693); dgat-2(hj44)* mutant animals. (C) A representative image showing partial LD localization of GFP. Asterisks indicate the position of nuclei. The cb5 C-terminal sequence substituted with four charged residues (red) is shown. (D) Red BODIPY-C12 staining of a representative larval stage L4 animal. Expanded LDs are marked by white arrowheads. Imaging conditions are identical to that used in Fig. 2. Bars, 10 μm. (E) Quantification of total volumes of BODIPY-positive structures that were >3 μm in diameter in the second intestinal segment of larval stage L4 animals. Data for *daf-22* and *daf-22; dgat-2* were reproduced from Fig. 2 G and shown here for comparison. For each strain, a total of 20 animals were imaged at two independent times, except for *daf-22; Si[dgat-2::cb5$_{mut}$]; dgat-2* (n = 29). Data were plotted as means ± SEM. (F) Relative DAG acyltransferase (DGAT) activity of wild-type and variant murine DGAT2 in yeast cell extracts. All variant DGAT2 proteins were expressed at comparable levels as shown in the Western blot. Data were obtained from duplicate assays of two independent experiments and normalized to bar 2. Means ± SEM. Asterisk shows no significant difference in one-way analysis of variance with Neuman-Keuls after testing. IB, immunoblot; WT, wild type.

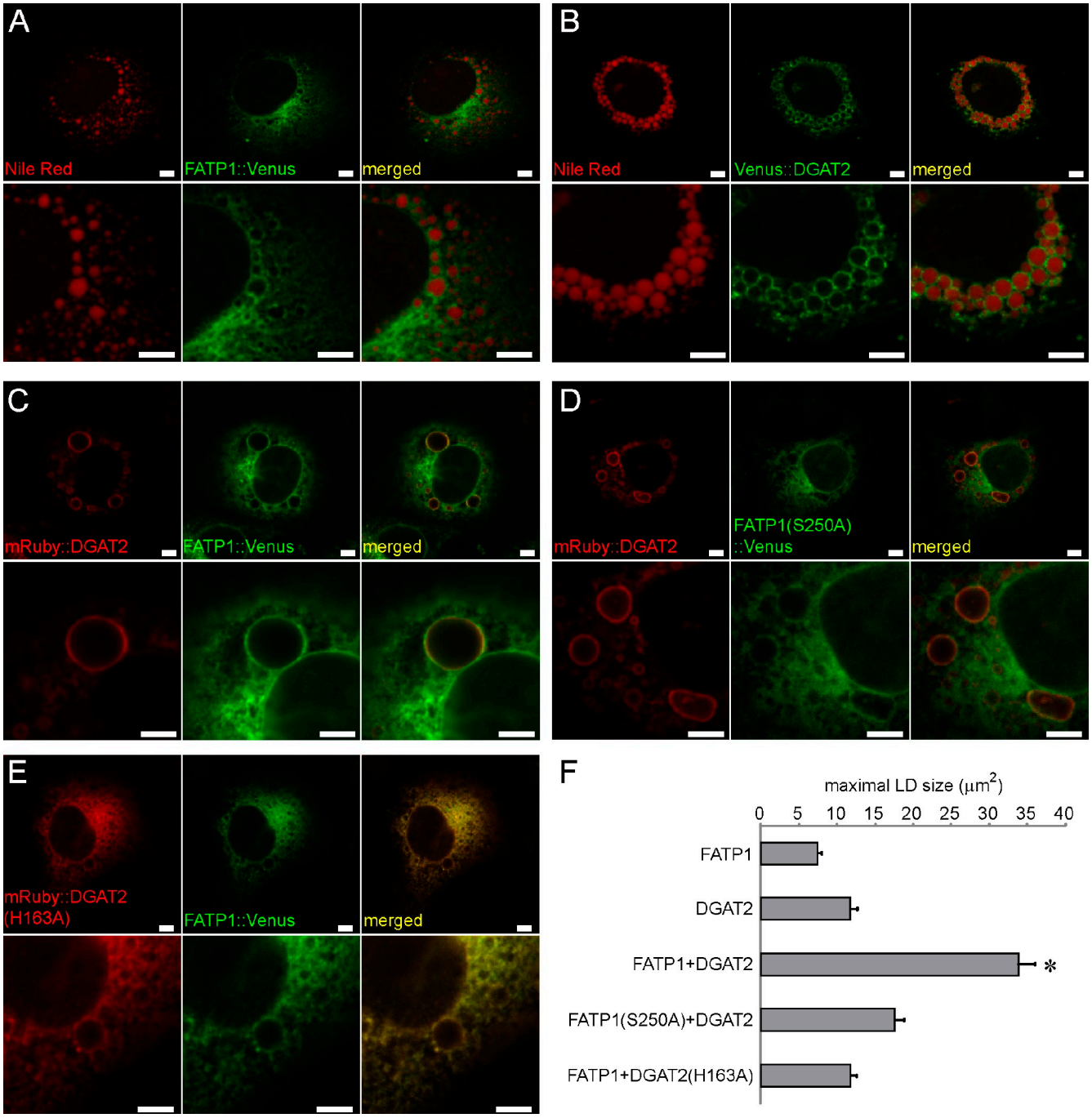

Figure 8. **FATP1 and DGAT2 act in concert to promote LD expansion in mammalian cells.** (A–E) COS7 cells were transfected with indicated FATP1 and/or DGAT2 constructs. Images were taken after incubation of transfected cells with oleic acid for 16–18 h. LDs were stained with Nile red. FATP1(S250A) and DGAT2(H163A) are catalytic dead mutants. Bars, 5 µm. (F) Quantification of maximal LD size (area in micrometers squared) in 30 transfected cells. Data were plotted as means ± SEM. *, $P < 0.001$ in *t* test between FATP1 + DGAT2 versus all other samples.

each other (Fig. 3 E). Therefore, preferential association of wild-type FATP1 and DGAT2 is highly specific (Fig. 3, C and E) and may indeed stabilize the docking of LDs to the ER.

We used a split GFP approach to further probe the spatial relationship between FATP1 and DGAT2 in mammalian cells. The GFP1–10 and GFP11 fragments can associate to reconstitute full-length GFP when they come into contact with each other, which can be facilitated by their fusion partners (Cabantous et al., 2005). In oleic acid–loaded COS7 cells, no signals were detected when GFP11 was coexpressed with GFP1–10 or GFP1–10::DGAT2 (Fig. 9, A and B). Coexpression of FATP1::GFP11 with GFP1–10 yielded signals in the ER (Fig. 9 C). In contrast, reconstituted GFP gave strong fluorescence signals around LDs when FATP1::GFP11 and GFP1–10::DGAT2 were coexpressed (Fig. 9 D). Our results indicate that FATP1 and DGAT2 are in close proximity of each other at the ER–LD interface. We conclude that FATP1 and DGAT2 act in concert to promote LD expansion at the ER–LD interface in an evolutionarily conserved manner.

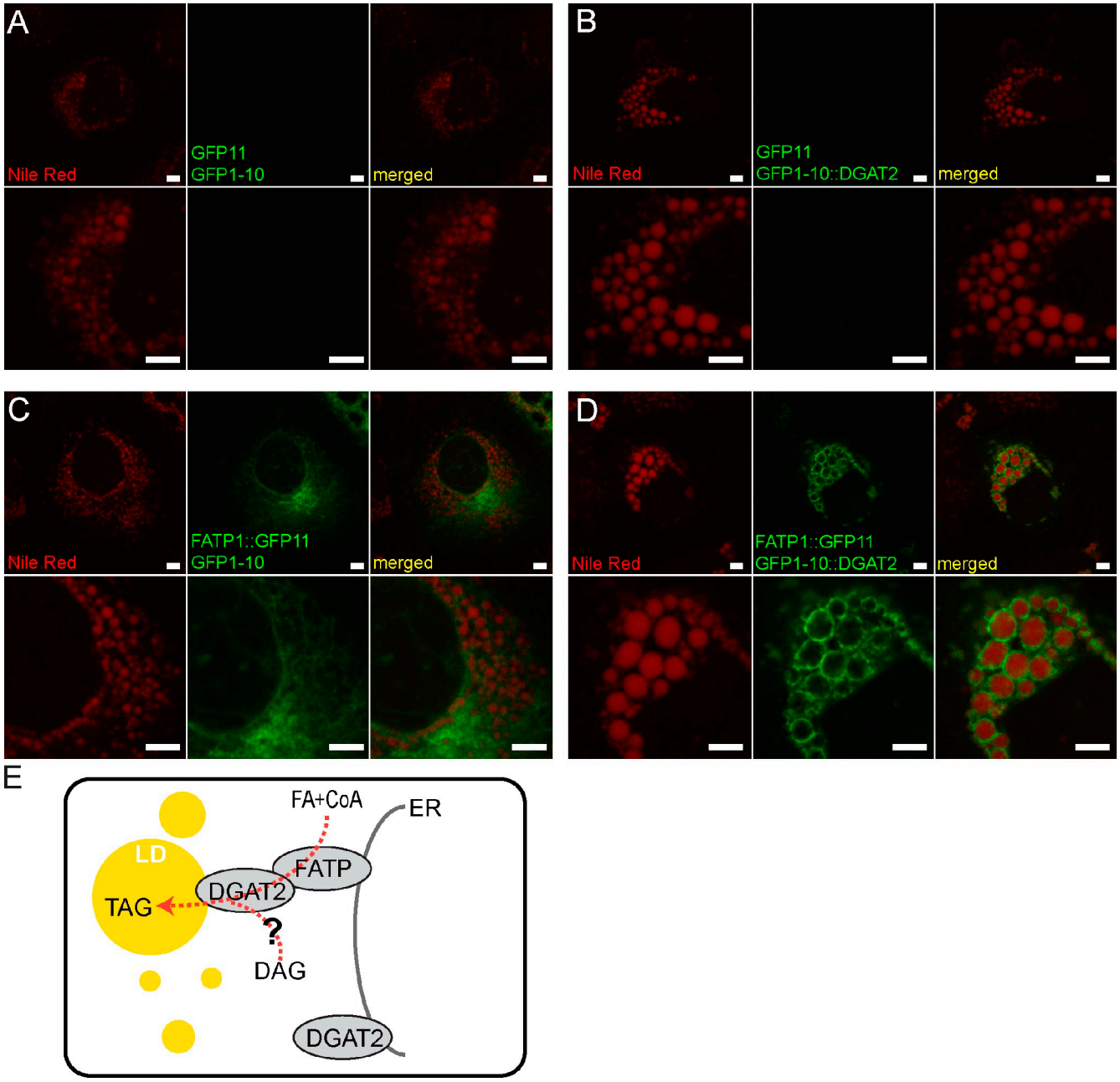

Figure 9. **FATP1 and DGAT2 at the ER–LD interface.** (A–D) COS7 cells were transfected with indicated GFP1–10 and GFP11 constructs. Images were taken after incubation of transfected cells with oleic acid for 16–18 h. LDs were stained with Nile red. Bars, 5 µm. (E) A model for LD expansion facilitated by the FATP1–DGAT2 triglyceride synthesis complex. DGAT2 has also been found at the ER in mammalian cells. FA, fatty acid; FATP, fatty acid transport protein; TAG, triglyceride.

Discussion

Close association of LDs with the ER has been observed (Blanchette-Mackie et al., 1995; Robenek et al., 2009), but the molecular mechanisms that enable their physical and functional coupling are not known. In this paper, we combine genetic, biochemical, and imaging approaches to demonstrate that a conserved FATP1–DGAT2 complex acts at the ER–LD interface to promote TAG synthesis and LD expansion.

FATP1 belongs to a large family of acyl-CoA synthetases that conjugates CoA to free fatty acid of various chain lengths, and it has been proposed that functional specificity of acyl-CoA synthetases may derive from their subcellular localization and interacting downstream partners (Ellis et al., 2010). Here, we provide a clear example of how this is achieved for FATP1 by identifying DGAT2 as its physical and functional partner in facilitating LD expansion through TAG synthesis. The physical interaction between FATP1 and DGAT2 and the distinct subcellular localization of their *C. elegans* orthologues prompt us to propose a model in which FATP1 and DGAT2 form a triglyceride synthesis protein complex that links LDs to the ER (Fig. 9 E). This complex fulfills two important functions: (1) coupling of

acyl-CoA synthesis in the ER to TAG synthesis on the LD surface; (2) deposition of newly synthesized TAG into the LD core. We further demonstrated that functional coupling of FATP1 and DGAT2 is evolutionarily conserved in mammalian cells.

The FATP1–DGAT2 complex defines a molecular link between the ER and LDs for the first time. The ER appears to use distinct macromolecular complexes to physically interact with other intracellular organelles. For example, the Mitofusin complex and the ER–mitochondria encounter structure complex have been shown to tether the ER to mitochondria (de Brito and Scorrano, 2008; Kornmann et al., 2009). Loss of Mitofusin 2 or components of the ER–mitochondria encounter structure complex disrupts the ER and/or mitochondrial morphology (de Brito and Scorrano, 2008; Kornmann et al., 2009). However, the ER morphology in mutant worms that lack ACS-22/FATP1 or DGAT-2 is normal, which suggests that the FATP1–DGAT2 complex is not required to maintain the structural integrity of the ER.

Although DGAT2 was originally assigned as a microsomal (ER) enzyme through biochemical fractionation experiments (Cases et al., 1998; Stone et al., 2006), it can also localize to mitochondrial-associated membranes and LDs upon lipid loading in mammalian cells (Kuerschner et al., 2008; Stone et al., 2009; McFie et al., 2011). Association with phospholipid bilayers by mouse DGAT2 has been attributed to its two predicted transmembrane segments, whereas discrete elements at its C terminus appeared to be necessary but not sufficient for LD association (McFie et al., 2011). The budding yeast orthologue of DGAT2, Dga1p, is strongly enriched in LDs in biochemical experiments (Sorger and Daum, 2002). It is therefore intriguing that mammalian DGAT2 has not been found broadly in LD proteomes. Perhaps the purification procedures were not amenable to preserving DGAT2 association with LDs. This may be caused in part by the interaction of DGAT2 with multiple ER resident proteins (see next paragraph). Nevertheless, our imaging data on DGAT2 in *C. elegans* and mammalian cells strongly suggest that DGAT2 can stably reside on the LD surface in vivo (Fig. 4 D, Fig. 8 B, and Fig. S5). More importantly, ER-tethered DGAT2 cannot substitute for LD-associated DGAT2 in promoting LD expansion (Fig. 7). Our results clearly demonstrate the physiological significance of LD-associated DGAT2.

A multisubunit protein complex for TAG synthesis had been isolated from rat intestinal villus cells, which contained acyl-CoA synthetase, acyl-CoA acyltransferase, monoacylglycerol acyltransferase, and DGAT activities (Manganaro and Kuksis, 1985; Lehner and Kuksis, 1995). It is plausible that FATP1 is responsible for the acyl-CoA synthetase activity in this complex. Additional proteins that are required for synthesis and modification of fatty acid and other lipid precursors of TAG may also be present in the FATP1–DGAT2 complex. For example, the steroyl-CoA desaturase SCD1, which catalyzes the desaturation of saturated fatty acids, was reported to associate with DGAT2 (Man et al., 2006).

TAG synthesis involves the conjugation of fatty acyl-CoA to DAG. DAG can be synthesized in the ER by phosphatidic acid phosphatases, such as Pah1p in budding yeast and Lipin-1 in metazoans (Reue and Brindley, 2008; Karanasios et al., 2010; Han et al., 2012). DAG has also been detected in purified LDs (Kuerschner et al., 2008), possibly the result of lipases such as adipose triglyceride lipase, and it is conceivable that DGAT2 on the LD surface may have direct access to such a pool of DAG. Furthermore, specific isoforms of Lipin-1 have been found at LDs (Valdearcos et al., 2011; Wang et al., 2011). Our model does not address the spatial distribution of the immediate precursors of DAG that are synthesized by enzymes in the Kennedy pathway or the monoacylglycerol pathway, which are classically regarded as microsomal (Coleman and Lee, 2004; Yen et al., 2008). It is plausible that dedicated proteins are responsible for transporting DAG and its precursors to the ER–LD interface. Alternatively, such precursors may be channeled through membrane connections between the ER and LDs.

The TAG content of LDs can be modulated by de novo TAG synthesis and reesterification of free fatty acids from lipolysis at the LD surface (Brooks et al., 1982). Although we favor a role for the FATP1–DGAT2 complex in channeling acyl-CoA from the ER and synthesizing TAG at the ER–LD interface, we cannot rule out its involvement in recycling hydrolyzed free fatty acids. It will be interesting to determine whether the assembly or activity of the FATP1–DGAT2 complex is responsive to lipolysis in future studies.

It has been proposed that LDs emerge from the ER through accumulation of neutral lipids between the phospholipid bilayer of the ER and subsequent pinching of the bulged ER with the neutral lipid core (Martin and Parton, 2006; Ploegh, 2007). Our study adds insight into how LDs expand and grow. We present evidence that preexisting LDs can expand by TAG synthesis and deposition through reengagement with the ER via the FATP1–DGAT2 complex in *C. elegans* and mammalian cells. In budding yeast, LDs appear to remain connected with the ER (Jacquier et al., 2011). Therefore, TAG synthesized in the ER can be partitioned to the LD core without invoking specific protein transporters. It is probable that LD expansion is facilitated by multiple parallel mechanisms. The relative dominance of each mechanism may be dictated by substrate availability and cellular context.

Materials and methods

Strains and transgenes

The wild-type strain was Bristol N2. All animals were raised at 20°C. The following alleles and transgenes were used: LGII, *daf-22(ok693)*; LGV, *dgat-2(hj44)*; and LGX, *acs-22(hj23)*, *acs-22(hj24)*, *acs-22(hj25)*, *acs-22(hj26)*, *acs-22(hj36)*, *hjIs14[vha-6p::GFP::C34B2.10(SP12)::unc-54 3′UTR]* (generated by microparticle bombardment and outcrossed four times with N2), *hjSi29[vha-6p::acs-22 cDNA::GFP-TEV-3×FLAG::let-858 3′ UTR] IV*, *hjSi56[vha-6p::3×FLAG-TEV-GFP::dgat-2::let-858 3′UTR] IV*, *hjSi61[vha-6p::mKO2:: C34B2.10(SP12)::let-858 3′UTR] II*, *hjSi62[vha-6p::3×FLAG-TEV-mRuby::dgat-2::let-858 3′UTR] II*, *hjSi76[vha-6p::3×FLAG-TEV-GFP::dgat-2::cb5 C terminus::let-858 3′UTR] IV*, and *hjSi87[vha-6p::3×FLAG-TEV-GFP::dgat-2::cb5 C terminus$_{mut}$::let-858 3′UTR] IV*.

Single-copy transgenes were generated as previously described (Frøkjaer-Jensen et al., 2008) using the direct injection protocol. The targeting plasmid (50 ng/µl) was injected with 50 ng/µl pJL43.1 (*Pglh-2::MosTase::glh-2 3′ UTR*) and coinjection markers into EG4322 or EG5003 for transgene insertion into LGII or LGIV, respectively. Transgenic strains were outcrossed at least two times with N2.

Genetic screens

The five *acs-22* alleles were isolated in a genetic screen for suppressors of the expanded LD phenotype of *daf-22(ok693)* mutants. Using a single nucleotide polymorphism–based mapping strategy with the Hawaiian *C. elegans* isolate CB4856 (Davis et al., 2005), we mapped *hj23* to LGX between haw105601 and snp_Y81B9A[4]. Based on the annotation of genes in the 800-kb region, we chose to sequence all exons and exon/intron junction of *acs-22* and identified a single C to T mutation that introduced a T603I substitution in animals carrying the *hj23* allele. Sequencing of four other alleles in the same complementation group, *hj24*, *hj25*, *hj26*, and *hj36*, revealed additional mutations in *acs-22*. The *daf-22(ok693); acs-22(hj26)* mutant could be rescued by an *acs-22p::acs-22::SL2-gfp* transgene.

From a genetic screen for suppressors of the expanded LD phenotype of *daf-22(ok693); hjSi29[acs-22::gfp]; acs-22(hj26)* mutants, we isolated mutant alleles in the *acs-22* coding region of the single-copy transgene as well as others that did not map to the transgene. We had previously determined that F59A1.10 RNAi could suppress LD expansion in *daf-22(ok693)* animals. Therefore, we sought alleles in F59A1.10 in the mutant allele collection by directly sequencing the exons and introns of F59A1.10 and recovered *hj44*. We renamed F59A1.10 as *dgat-2* for its sequence and functional homology to mammalian DGAT2. The *hj44* allele encodes a G296E substitution in *C. elegans* DGAT-2. The *daf-22(ok693); dgat-2(hj44)* mutant could be rescued by a *dgat-2p::dgat-2::SL2-gfp* transgene.

Lipid analyses

Lipid analyses involving total lipid extraction, TLC, and gas chromatography–mass spectrometry were performed to compare relative changes of major lipid species, quantify TAG levels, and profile fatty acid compositions. Procedures were essentially the same as previously described (Zhang et al., 2010a). For TAG quantification, the number of L4 animals for each replicate sample was scaled down from 24,000 to 12,000. Quantitation of fatty acid uptake using ^{13}C isotope labeling was performed as previously described using the mass spectroscopy–selective ion monitoring mode (Perez and Van Gilst, 2008). *Escherichia coli* OP50 was grown in uracil-supplemented Spectra 9-U medium or Spectra 9-C medium (^{13}C, 98%) obtained from Cambridge Isotope Laboratories. Lipid was extracted from 30,000 synchronized L4 larval animals for each sample.

Postfix Oil red O staining

Postfix Oil red O staining was performed essentially as previously described (O'Rourke et al., 2009). Animals were fixed in 1% formaldehyde/PBS for 10 min at 22°C in 15-ml glass conical tubes. Samples were frozen on dry ice and thawed for three cycles. After extensive washing with PBS, animals were stained with Oil red O in 60% isopropanol for 30 min at 22°C and washed and destained for 15 min in PBS at the same temperature. Images were acquired in bright field with the same settings on a microscope (Axiovert; Carl Zeiss) equipped with a 40×, NA 0.6 air objective (LD Achroplan; Carl Zeiss) and a camera (AxioCam HR; Carl Zeiss) controlled by the AxioVision software (Carl Zeiss).

Confocal imaging and size measurement of LDs

Confocal imaging and size measurement of red BODIPY-stained LD on late-stage L4 animals were conducted essentially the same as previously described (Zhang et al., 2010a). Images were acquired on a confocal microscope (LSM 510; Carl Zeiss) using a 40×, NA 1.2 water C-Apochromat objective. Optical sections were taken at 0.45-µm intervals, and z stacks of 9.0 µm were exported to Imaris 6.2.1 (Bitplane) for identification, annotation, and measurement of diameter of all BODIPY-labeled structures. Spectrally unmixed images were first acquired on a confocal microscope (LSM 710; Carl Zeiss) in λ mode using a 40×, NA 1.2 water C-Apochromat objective and GFP and autofluorescence unmixed using the ZEN software (Carl Zeiss).

Quantitation of colocalization of fluorescent signals

Images were taken on larval stage L4 worms using a confocal microscope (LSM 710) with a 40×, NA 1.2 water C-Apochromat objective. For each animal, GFP and mRuby fluorescence images were collected in multitrack mode to prevent leakage. A Pearson's coefficient was calculated for each image based on pixels of interest (Manders et al., 1992). A threshold in the mRuby channel of the upper 5% of all pixels was sufficient for masking only relevant pixels across worms. To prevent underestimation of the colocalization coefficients, images with pronounced autofluorescent signals appearing as filled spherical structures were excluded (see Fig. 4 for a comparison of autofluorescent structures and LDs).

Photobleaching

Photobleaching experiments were performed on larval stage L4 animals on a confocal microscope (LSM 710) using a 40×, NA 1.2 water C-Apochromat objective and controlled by the ZEN software. For each animal, one or more areas of 2 µm in diameter were selected. For Fig. 5 H, a time series of the entire field (2,500–3,600 µm^2) was taken, and after the fifth frame, 10 cycles of photobleaching was performed using a 488-nm laser at maximum power. The time series continued until structures returned visibly with respect to neighboring unbleached regions or after 200 s of imaging. The fluorescence recovery of the bleached region was fit to an exponential after adjusting for the slow decay of fluorescence caused by imaging using areas of the image distant from the bleached region. At least eight photobleaching events were recorded for each strain. For Fig. 6 (A–F), a time series of the entire field (~4,900 µm^2) was taken, and 200 cycles of photobleaching was performed after the fifth frame using a 488-nm laser at maximum power. The time series was collected for another 30 s. Photobleaching curves that showed 65% or more absolute loss of fluorescence postbleach were normalized and collected into Fig. 6 G.

Electron microscopy

For gold immunolabeling of GFP, dissected *C. elegans* intestines were fixed with 2% formaldehyde and permeabilized with PBS + 0.1% Triton X-100. Samples were blocked in PBS + 1% BSA and incubated with anti-GFP antibody followed by goat anti–mouse super small gold (Electron Microscopy Sciences). Samples were then fixed with 2.5% glutaraldehyde in PBS (10 min) and washed with distilled water, and gold staining signal was enhanced with a silver enhancement kit (Aurion). After washing with distilled water, samples were postfixed in 1% OsO_4 containing 1.5% potassium ferrocyanide in PBS for 30 min at room temperature and washed with distilled water. Samples were dehydrated in ethanol, embedded in epoxy resin (room temperature for 2 d), and polymerized (60°C for 2 d). Sections (50–70 nm thick) were cut and transferred to Formvar-coated grids and stained with aqueous uranyl acetate and lead citrate. Sections were analyzed on an electron microscope (80 kV; Tecnai Spirit; FEI).

Immunoprecipitation

Human epithelial HeLa cells and human embryonic kidney 293 cells were cultured in 6-well plates and transfected with 4 µg per well of expression plasmids that were based on pcDNA5 (Invitrogen) using Lipofectamine 2000 (Invitrogen). Cells were harvested 24 h after transfection, and whole-cell lysates were prepared using MAPK buffer (10 mM Tris-HCl, pH 8.0, 50 mM NaCl, 1 mM EDTA, 1% NP-40, and protease inhibitors [Complete; Roche]). Immunoprecipitations with agarose beads conjugated with anti-FLAG were performed at 4°C for 2.5 h. In vitro translation was performed using a coupled reticulocyte lysate system (TNT; Promega). The lysates containing in vitro translated proteins were diluted by 1 vol MAPK buffer before immunoprecipitation. Protein complexes were eluted by boiling in 3× SDS loading buffer (mammalian cell lysates coimmunoprecipitation) or with 0.2 mg/ml 3× FLAG peptide at 4°C for 1 h (in vitro translated proteins coimmunoprecipitation) before SDS-PAGE.

DGAT assay

DGAT activity was measured as described previously (Liu et al., 2010) with minor modifications. The assay was conducted in a buffer containing 150 mM Hepes-KOH, pH 7.0, 2.5 mM $MgCl_2$, 0.1 mg/ml BSA, 308 µM dioleoyl glycerol, and 15 µM [^{14}C]oleoyl-CoA (18 µCi/µmol) with 100 µg microsomal protein in a final volume of 200 µl. This assay mixture was incubated at 30°C for 10 min and quenched by addition of 4 ml chloroform/methanol (2:1). Nonlipid molecules were extracted by addition of 0.75 ml H_2O with thorough mixing. The aqueous phase was removed, and the organic phase was dried down under nitrogen. Lipids were reconstituted in 30 µl chloroform and resolved by TLC using a hexane/ether/acetic acid (80:20:1) mobile phase. The plate was analyzed using a phosphor storage screen, and the triglyceride band intensity was quantitated using ImageQuant Array software (GE Healthcare). Data presented are the mean of two independent microsome preps performed in duplicate and normalized to the Δ4 strain expressing the empty vector.

Yeast strains/plasmids

Wild-type *[MATa ADE2]* and Δ4 *[MATα are1-Δ::HIS3 are2-Δ::LEU2 dga1-Δ::KanMX4 lro1-Δ::TRP1 ADE2]* strains are previously described (Sandager et al., 2002). cDNAs encoding mRuby fluorescent protein and murine DGAT2 were cloned in frame into p426-GPD mRuby. CB5 and CB5 mutant tags were added to the C terminus of DGAT2 with no intervening sequence.

Antibodies

For Western blotting, monoclonal antibodies against the FLAG epitope (clone M2; Sigma-Aldrich; 1:1,000) and HA epitope (clone 3F10; Roche; 1:1,000), rabbit polyclonal antibodies against ACS-22 (amino acids 216–231; 1:300; YZ677; YenZym) and DGAT2 (NBP1-71700; Novus Biologicals; 1:500) were used. For immunoprecipitation, anti-FLAG M2 affinity gel (Sigma-Aldrich) was used.

Mammalian cells confocal imaging

COS7 cells were transfected with pcDNA3.1 (Invitrogen)-based expression plasmids using Lipofectamine (Invitrogen) in poly-D-lysine 4-well glass slides (CultureSlides; BD). Oleic acid (Nu-Chek Prep) conjugated with BSA was added to cells 8 h after transfection at a final concentration of 400 µM. Cells were incubated for 16 h before fixation with 4% formaldehyde (22°C for 15 min). Fixed cells were washed three times with PBS, once with 0.1% Triton X-100 in PBS (22°C for 2 min), and then two times with PBS. LDs were visualized by adding 100 ng/ml Nile red in PBS to the cells (22°C for 5 min). Cells were washed once with PBS before mounting with VECTASHIELD with DAPI (Vector Laboratories). Images were acquired on a confocal microscope (LSM 710) in channel mode using a 40×, NA 1.2 water C-Apochromat objective and 3 or 8× zoom and controlled by the ZEN software. GFP was excited with a 488-nm laser (4%), and mRuby and Nile red were excited with a 561-nm laser (5%).

Online supplemental material

Fig. S1 shows molecular lesions in the *acs-22* gene. Fig. S2 shows that ACS-22 acts cell autonomously to promote LD expansion. Fig. S3 shows LD expansion in mutant animals carrying *acs-22* or *dgat-2* transgenes. Fig. S4 shows ACS-22 and DGAT-2 are ER and LD resident proteins, respectively, by FRAP analysis. Fig. S5 shows colocalization of DGAT2 and Perilipin2. Table S1 shows results of knockdown of acyl-CoA synthetases by RNAi. Online supplemental material is available at http://www.jcb.org/cgi/content/full/jcb.201201139/DC1.

We thank Yan Hao for generating *hjSi62*, Marc Van Gilst and Carissa Perez Olsen for advice on ^{13}C isotope labeling experiments, Perry Bickel for protocols, and Robb Krumlauf for critical reading of the manuscript.

This work was supported by the Stowers Institute for Medical Research (to H.Y. Mak) and National Institutes of Health grant RO1 2R56DK56084 (to R.V. Farese Jr.).

Author contributions: N. Xu was responsible for Fig. 1 (I and J), Fig. 2 (D and G), Fig. 3, Fig. 4, Fig. 5 (A–F), Fig. 6 (A–F and H–J), Fig. 7 (A–E), Fig. 8, Fig. 9, Fig. S1, Fig. S2, Fig. S3 (C–J), Fig. S5, and Table S1. S.O. Zhang was responsible for Fig. 1 G, Fig. 2 (A–C and E–G), and Fig. S3 (A and B). R.A. Cole was responsible for Fig. 1 (A–F and H) and Table S1. S.A. McKinney was responsible for Fig. 5 (G and H), Fig. 6 G, and Fig. S4. F. Guo was responsible for Fig. 6 (H–J). J.T. Haas and R.V. Farese Jr. were responsible for Fig. 7 F. H.Y. Mak, N. Xu, S.O. Zhang, and R.A. Cole conducted genetic screens. N. Xu and R.A. Cole performed genetic mapping and molecular cloning of mutants. S. Bobba contributed analysis tools for Fig. 1 H. All authors participated in data analysis. H.Y. Mak conceived the project and wrote the manuscript.

Submitted: 25 January 2012
Accepted: 31 July 2012

References

Blanchette-Mackie, E.J., N.K. Dwyer, T. Barber, R.A. Coxey, T. Takeda, C.M. Rondinone, J.L. Theodorakis, A.S. Greenberg, and C. Londos. 1995. Perilipin is located on the surface layer of intracellular lipid droplets in adipocytes. *J. Lipid Res.* 36:1211–1226.

Brooks, B., J.R. Arch, and E.A. Newsholme. 1982. Effects of hormones on the rate of the triacylglycerol/fatty acid substrate cycle in adipocytes and epididymal fat pads. *FEBS Lett.* 146:327–330. http://dx.doi.org/10.1016/0014-5793(82)80945-9

Cabantous, S., T.C. Terwilliger, and G.S. Waldo. 2005. Protein tagging and detection with engineered self-assembling fragments of green fluorescent protein. *Nat. Biotechnol.* 23:102–107. http://dx.doi.org/10.1038/nbt1044

Cases, S., S.J. Smith, Y.W. Zheng, H.M. Myers, S.R. Lear, E. Sande, S. Novak, C. Collins, C.B. Welch, A.J. Lusis, et al. 1998. Identification of a gene encoding an acyl CoA:diacylglycerol acyltransferase, a key enzyme in triacylglycerol synthesis. *Proc. Natl. Acad. Sci. USA*. 95:13018–13023. http://dx.doi.org/10.1073/pnas.95.22.13018

Cases, S., S.J. Stone, P. Zhou, E. Yen, B. Tow, K.D. Lardizabal, T. Voelker, and R.V. Farese Jr. 2001. Cloning of DGAT2, a second mammalian diacylglycerol acyltransferase, and related family members. *J. Biol. Chem.* 276:38870–38876. http://dx.doi.org/10.1074/jbc.M106219200

Coe, N.R., A.J. Smith, B.I. Frohnert, P.A. Watkins, and D.A. Bernlohr. 1999. The fatty acid transport protein (FATP1) is a very long chain acyl-CoA synthetase. *J. Biol. Chem.* 274:36300–36304. http://dx.doi.org/10.1074/jbc.274.51.36300

Coleman, R.A., and D.P. Lee. 2004. Enzymes of triacylglycerol synthesis and their regulation. *Prog. Lipid Res.* 43:134–176. http://dx.doi.org/10.1016/S0163-7827(03)00051-1

Davis, M.W., M. Hammarlund, T. Harrach, P. Hullett, S. Olsen, and E.M. Jorgensen. 2005. Rapid single nucleotide polymorphism mapping in *C. elegans*. *BMC Genomics*. 6:118. http://dx.doi.org/10.1186/1471-2164-6-118

de Brito, O.M., and L. Scorrano. 2008. Mitofusin 2 tethers endoplasmic reticulum to mitochondria. *Nature*. 456:605–610. http://dx.doi.org/10.1038/nature07534

Ellis, J.M., J.L. Frahm, L.O. Li, and R.A. Coleman. 2010. Acyl-coenzyme A synthetases in metabolic control. *Curr. Opin. Lipidol.* 21:212–217. http://dx.doi.org/10.1097/MOL.0b013e32833884bb

Farese, R.V., Jr., and T.C. Walther. 2009. Lipid droplets finally get a little R-E-S-P-E-C-T. *Cell*. 139:855–860. http://dx.doi.org/10.1016/j.cell.2009.11.005

Frøkjaer-Jensen, C., M.W. Davis, C.E. Hopkins, B.J. Newman, J.M. Thummel, S.P. Olesen, M. Grunnet, and E.M. Jorgensen. 2008. Single-copy insertion of transgenes in *Caenorhabditis elegans*. *Nat. Genet.* 40:1375–1383. http://dx.doi.org/10.1038/ng.248

Goodman, J.M. 2009. Demonstrated and inferred metabolism associated with cytosolic lipid droplets. *J. Lipid Res.* 50:2148–2156. http://dx.doi.org/10.1194/jlr.R001446

Grönke, S., A. Mildner, S. Fellert, N. Tennagels, S. Petry, G. Müller, H. Jäckle, and R.P. Kühnlein. 2005. Brummer lipase is an evolutionary conserved fat storage regulator in *Drosophila*. *Cell Metab.* 1:323–330. http://dx.doi.org/10.1016/j.cmet.2005.04.003

Hall, A.M., A.J. Smith, and D.A. Bernlohr. 2003. Characterization of the Acyl-CoA synthetase activity of purified murine fatty acid transport protein 1. *J. Biol. Chem.* 278:43008–43013. http://dx.doi.org/10.1074/jbc.M306575200

Han, S., S. Bahmanyar, P. Zhang, N. Grishin, K. Oegema, R. Crooke, M. Graham, K. Reue, J.E. Dixon, and J.M. Goodman. 2012. Nuclear envelope phosphatase 1-regulatory subunit 1 (formerly TMEM188) is the metazoan Spo7p ortholog and functions in the lipin activation pathway. *J. Biol. Chem.* 287:3123–3137. http://dx.doi.org/10.1074/jbc.M111.324350

Harris, C.A., J.T. Haas, R.S. Streeper, S.J. Stone, M. Kumari, K. Yang, X. Han, N. Brownell, R.W. Gross, R. Zechner, and R.V. Farese Jr. 2011. DGAT enzymes are required for triacylglycerol synthesis and lipid droplets in adipocytes. *J. Lipid Res.* 52:657–667. http://dx.doi.org/10.1194/jlr.M013003

Hisanaga, Y., H. Ago, N. Nakagawa, K. Hamada, K. Ida, M. Yamamoto, T. Hori, Y. Arii, M. Sugahara, S. Kuramitsu, et al. 2004. Structural basis of the substrate-specific two-step catalysis of long chain fatty acyl-CoA synthetase dimer. *J. Biol. Chem.* 279:31717–31726. http://dx.doi.org/10.1074/jbc.M400100200

Honsho, M., J.Y. Mitoma, and A. Ito. 1998. Retention of cytochrome b5 in the endoplasmic reticulum is transmembrane and luminal domain-dependent. *J. Biol. Chem.* 273:20860–20866. http://dx.doi.org/10.1074/jbc.273.33.20860

Jacquier, N., V. Choudhary, M. Mari, A. Toulmay, F. Reggiori, and R. Schneiter. 2011. Lipid droplets are functionally connected to the endoplasmic reticulum in *Saccharomyces cerevisiae*. *J. Cell Sci.* 124:2424–2437. http://dx.doi.org/10.1242/jcs.076836

Kage-Nakadai, E., H. Kobuna, M. Kimura, K. Gengyo-Ando, T. Inoue, H. Arai, and S. Mitani. 2010. Two very long chain fatty acid acyl-CoA synthetase genes, acs-20 and acs-22, have roles in the cuticle surface barrier in *Caenorhabditis elegans*. *PLoS ONE*. 5:e8857. http://dx.doi.org/10.1371/journal.pone.0008857

Karanasios, E., G.S. Han, Z. Xu, G.M. Carman, and S. Siniossoglou. 2010. A phosphorylation-regulated amphipathic helix controls the membrane translocation and function of the yeast phosphatidate phosphatase. *Proc. Natl. Acad. Sci. USA*. 107:17539–17544. http://dx.doi.org/10.1073/pnas.1007974107

Kornmann, B., E. Currie, S.R. Collins, M. Schuldiner, J. Nunnari, J.S. Weissman, and P. Walter. 2009. An ER-mitochondria tethering complex revealed by a synthetic biology screen. *Science*. 325:477–481. http://dx.doi.org/10.1126/science.1175088

Kuerschner, L., C. Moessinger, and C. Thiele. 2008. Imaging of lipid biosynthesis: how a neutral lipid enters lipid droplets. *Traffic*. 9:338–352. http://dx.doi.org/10.1111/j.1600-0854.2007.00689.x

Lehner, R., and A. Kuksis. 1995. Triacylglycerol synthesis by purified triacylglycerol synthetase of rat intestinal mucosa. Role of acyl-CoA acyltransferase. *J. Biol. Chem.* 270:13630–13636. http://dx.doi.org/10.1074/jbc.270.23.13630

Lewis, S.E., L.L. Listenberger, D.S. Ory, and J.E. Schaffer. 2001. Membrane topology of the murine fatty acid transport protein 1. *J. Biol. Chem.* 276:37042–37050. http://dx.doi.org/10.1074/jbc.M105556200

Listenberger, L.L., X. Han, S.E. Lewis, S. Cases, R.V. Farese Jr., D.S. Ory, and J.E. Schaffer. 2003. Triglyceride accumulation protects against fatty acid-induced lipotoxicity. *Proc. Natl. Acad. Sci. USA*. 100:3077–3082. http://dx.doi.org/10.1073/pnas.0630588100

Liu, Q., R.M. Siloto, and R.J. Weselake. 2010. Role of cysteine residues in thiol modification of acyl-CoA:diacylglycerol acyltransferase 2 from yeast. *Biochemistry*. 49:3237–3245. http://dx.doi.org/10.1021/bi9020499

Mak, H.Y. 2012. Lipid droplets as fat storage organelles in *Caenorhabditis elegans*: Thematic Review Series: Lipid Droplet Synthesis and Metabolism: from Yeast to Man. *J. Lipid Res.* 53:28–33. http://dx.doi.org/10.1194/jlr.R021006

Man, W.C., M. Miyazaki, K. Chu, and J. Ntambi. 2006. Colocalization of SCD1 and DGAT2: implying preference for endogenous monounsaturated fatty acids in triglyceride synthesis. *J. Lipid Res.* 47:1928–1939. http://dx.doi.org/10.1194/jlr.M600172-JLR200

Manders, E.M., J. Stap, G.J. Brakenhoff, R. van Driel, and J.A. Aten. 1992. Dynamics of three-dimensional replication patterns during the S-phase, analysed by double labelling of DNA and confocal microscopy. *J. Cell Sci.* 103:857–862.

Manganaro, F., and A. Kuksis. 1985. Rapid isolation of a triacylglycerol synthetase complex from rat intestinal mucosa. *Can. J. Biochem. Cell Biol.* 63:107–114. http://dx.doi.org/10.1139/o85-016

Martin, S., and R.G. Parton. 2006. Lipid droplets: a unified view of a dynamic organelle. *Nat. Rev. Mol. Cell Biol.* 7:373–378. http://dx.doi.org/10.1038/nrm1912

McFie, P.J., S.L. Banman, S. Kary, and S.J. Stone. 2011. Murine diacylglycerol acyltransferase-2 (DGAT2) can catalyze triacylglycerol synthesis and promote lipid droplet formation independent of its localization to the endoplasmic reticulum. *J. Biol. Chem.* 286:28235–28246. http://dx.doi.org/10.1074/jbc.M111.256008

O'Rourke, E.J., A.A. Soukas, C.E. Carr, and G. Ruvkun. 2009. *C. elegans* major fats are stored in vesicles distinct from lysosome-related organelles. *Cell Metab.* 10:430–435. http://dx.doi.org/10.1016/j.cmet.2009.10.002

Perez, C.L., and M.R. Van Gilst. 2008. A 13C isotope labeling strategy reveals the influence of insulin signaling on lipogenesis in *C. elegans. Cell Metab.* 8:266–274. http://dx.doi.org/10.1016/j.cmet.2008.08.007

Ploegh, H.L. 2007. A lipid-based model for the creation of an escape hatch from the endoplasmic reticulum. *Nature*. 448:435–438. http://dx.doi.org/10.1038/nature06004

Reue, K., and D.N. Brindley. 2008. Thematic Review Series: Glycerolipids. Multiple roles for lipins/phosphatidate phosphatase enzymes in lipid metabolism. *J. Lipid Res.* 49:2493–2503. http://dx.doi.org/10.1194/jlr.R800019-JLR200

Richards, M.R., L.L. Listenberger, A.A. Kelly, S.E. Lewis, D.S. Ory, and J.E. Schaffer. 2003. Oligomerization of the murine fatty acid transport protein 1. *J. Biol. Chem.* 278:10477–10483. http://dx.doi.org/10.1074/jbc.M212469200

Robenek, H., I. Buers, O. Hofnagel, M.J. Robenek, D. Troyer, and N.J. Severs. 2009. Compartmentalization of proteins in lipid droplet biogenesis. *Biochim. Biophys. Acta*. 1791:408–418. http://dx.doi.org/10.1016/j.bbalip.2008.12.001

Rolls, M.M., D.H. Hall, M. Victor, E.H. Stelzer, and T.A. Rapoport. 2002. Targeting of rough endoplasmic reticulum membrane proteins and ribosomes in invertebrate neurons. *Mol. Biol. Cell*. 13:1778–1791. http://dx.doi.org/10.1091/mbc.01-10-0514

Sandager, L., M.H. Gustavsson, U. Ståhl, A. Dahlqvist, E. Wiberg, A. Banas, M. Lenman, H. Ronne, and S. Stymne. 2002. Storage lipid synthesis is non-essential in yeast. *J. Biol. Chem.* 277:6478–6482. http://dx.doi.org/10.1074/jbc.M109109200

Schaffer, J.E., and H.F. Lodish. 1994. Expression cloning and characterization of a novel adipocyte long chain fatty acid transport protein. *Cell*. 79:427–436. http://dx.doi.org/10.1016/0092-8674(94)90252-6

Schroeder, L.K., S. Kremer, M.J. Kramer, E. Currie, E. Kwan, J.L. Watts, A.L. Lawrenson, and G.J. Hermann. 2007. Function of the *Caenorhabditis elegans* ABC transporter PGP-2 in the biogenesis of a lysosome-related fat storage organelle. *Mol. Biol. Cell*. 18:995–1008. http://dx.doi.org/10.1091/mbc.E06-08-0685

Skinner, J.R., T.M. Shew, D.M. Schwartz, A. Tzekov, C.M. Lepus, N.A. Abumrad, and N.E. Wolins. 2009. Diacylglycerol enrichment of endoplasmic reticulum or lipid droplets recruits perilipin 3/TIP47 during lipid storage and mobilization. *J. Biol. Chem.* 284:30941–30948. http://dx.doi.org/10.1074/jbc.M109.013995

Sorger, D., and G. Daum. 2002. Synthesis of triacylglycerols by the acyl-coenzyme A:diacyl-glycerol acyltransferase Dga1p in lipid particles of the yeast *Saccharomyces cerevisiae*. *J. Bacteriol.* 184:519–524. http://dx.doi.org/10.1128/JB.184.2.519-524.2002

Stahl, A., D.J. Hirsch, R.E. Gimeno, S. Punreddy, P. Ge, N. Watson, S. Patel, M. Kotler, A. Raimondi, L.A. Tartaglia, and H.F. Lodish. 1999. Identification of the major intestinal fatty acid transport protein. *Mol. Cell*. 4:299–308. http://dx.doi.org/10.1016/S1097-2765(00)80332-9

Stahl, A., J.G. Evans, S. Pattel, D. Hirsch, and H.F. Lodish. 2002. Insulin causes fatty acid transport protein translocation and enhanced fatty acid uptake in adipocytes. *Dev. Cell*. 2:477–488. http://dx.doi.org/10.1016/S1534-5807(02)00143-0

Stone, S.J., M.C. Levin, and R.V. Farese Jr. 2006. Membrane topology and identification of key functional amino acid residues of murine acyl-CoA:diacylglycerol acyltransferase-2. *J. Biol. Chem.* 281:40273–40282. http://dx.doi.org/10.1074/jbc.M607986200

Stone, S.J., M.C. Levin, P. Zhou, J. Han, T.C. Walther, and R.V. Farese Jr. 2009. The endoplasmic reticulum enzyme DGAT2 is found in mitochondria-associated membranes and has a mitochondrial targeting signal that promotes its association with mitochondria. *J. Biol. Chem.* 284:5352–5361. http://dx.doi.org/10.1074/jbc.M805768200

Stuhlsatz-Krouper, S.M., N.E. Bennett, and J.E. Schaffer. 1998. Substitution of alanine for serine 250 in the murine fatty acid transport protein inhibits long chain fatty acid transport. *J. Biol. Chem.* 273:28642–28650. http://dx.doi.org/10.1074/jbc.273.44.28642

Szymanski, K.M., D. Binns, R. Bartz, N.V. Grishin, W.P. Li, A.K. Agarwal, A. Garg, R.G. Anderson, and J.M. Goodman. 2007. The lipodystrophy protein seipin is found at endoplasmic reticulum lipid droplet junctions and is important for droplet morphology. *Proc. Natl. Acad. Sci. USA*. 104:20890–20895. http://dx.doi.org/10.1073/pnas.0704154104

Unger, R.H., and P.E. Scherer. 2010. Gluttony, sloth and the metabolic syndrome: a roadmap to lipotoxicity. *Trends Endocrinol. Metab.* 21:345–352. http://dx.doi.org/10.1016/j.tem.2010.01.009

Valdearcos, M., E. Esquinas, C. Meana, L. Gil-de-Gómez, C. Guijas, J. Balsinde, and M.A. Balboa. 2011. Subcellular localization and role of lipin-1 in human macrophages. *J. Immunol.* 186:6004–6013. http://dx.doi.org/10.4049/jimmunol.1003279

Voeltz, G.K., M.M. Rolls, and T.A. Rapoport. 2002. Structural organization of the endoplasmic reticulum. *EMBO Rep.* 3:944–950. http://dx.doi.org/10.1093/embo-reports/kvf202

Wang, H., J. Zhang, W. Qiu, G.S. Han, G.M. Carman, and K. Adeli. 2011. Lipin-1γ isoform is a novel lipid droplet-associated protein highly expressed in the brain. *FEBS Lett.* 585:1979–1984. http://dx.doi.org/10.1016/j.febslet.2011.05.035

Yen, C.L., S.J. Stone, S. Koliwad, C. Harris, and R.V. Farese Jr. 2008. Thematic review series: glycerolipids. DGAT enzymes and triacylglycerol biosynthesis. *J. Lipid Res.* 49:2283–2301. http://dx.doi.org/10.1194/jlr.R800018-JLR200

Zechner, R., P.C. Kienesberger, G. Haemmerle, R. Zimmermann, and A. Lass. 2009. Adipose triglyceride lipase and the lipolytic catabolism of cellular fat stores. *J. Lipid Res.* 50:3–21. http://dx.doi.org/10.1194/jlr.R800031-JLR200

Zhang, S.O., A.C. Box, N. Xu, J. Le Men, J. Yu, F. Guo, R. Trimble, and H.Y. Mak. 2010a. Genetic and dietary regulation of lipid droplet expansion in *Caenorhabditis elegans. Proc. Natl. Acad. Sci. USA*. 107:4640–4645. http://dx.doi.org/10.1073/pnas.0912308107

Zhang, S.O., R. Trimble, F. Guo, and H.Y. Mak. 2010b. Lipid droplets as ubiquitous fat storage organelles in *C. elegans. BMC Cell Biol.* 11:96. http://dx.doi.org/10.1186/1471-2121-11-96

Zhu, W., A. Cowie, G.W. Wasfy, L.Z. Penn, B. Leber, and D.W. Andrews. 1996. Bcl-2 mutants with restricted subcellular location reveal spatially distinct pathways for apoptosis in different cell types. *EMBO J.* 15:4130–4141.